Structural Engineering and Mechanics, *Vol. 48, No. 5 (2013) 587-613*
DOI: http://dx.doi.org/10.12989/sem.2013.48.5.587

A 3D co-rotational beam element for steel and RC framed structures

Xu Long*, Kang Hai Tan and Chi King Lee

School of Civil and Environmental Engineering, Nanyang Technological University, 50 Nanyang Avenue, Singapore 639798, Singapore

(Received February 19, 2013, Revised October 22, 2013, Accepted November 1, 2013)

Abstract. A 3-node 3D co-rotational beam element using vectorial rotational variables is employed to consider the geometric nonlinearity in 3D space. To account for shape versatility and reinforced concrete cross-sections, fibre model has been derived and conducted. Numerical integration over the cross-section is performed, considering both normal and shear stresses. In addition, the derivations associated with material nonlinearity are given in terms of elasto-plastic incremental stress-strain relationship for both steel and concrete. Steel reinforcement is treated as elasto-plastic material with Von Mises yield criterion. Compressive concrete behaviour is described by Modified Kent and Park model, while tensile stiffening effect is taken into account as well. Through several numerical examples, it is shown that the proposed 3D co-rotational beam element with fibre model can be used to simulate steel and reinforced concrete framed structures with satisfactory accuracy and efficiency.

Keywords: 3D co-rotational beam element; geometric nonlinearity; material nonlinearity; fibre model; steel structures; reinforced concrete structures

1. Introduction

For framed structures subjected to extreme loading such as an earthquake or a blast event, collapse takes place initially from the failures of some critical structural members, such as beams, columns and joints, which deform and fail before failure spreads to the entire structure. At the member level, it is important for finite element analysis to capture the characteristics of material yielding and large geometric deformation, so as to simulate the process of progressive collapse. Besides, the analysis should also model hardening property of materials as well as overall softening of structural response, as the structure is on the verge of collapse.

In terms of geometric nonlinearity, the efficient approaches of beam elements for large deformation analysis of frame structures can be generally classified into three types, that is, total Lagrangian (TL) formulation (Bathe and Bolourchi 1979, Schulz and Filippou 2001, Nanakorn and Vu 2006), updated Lagrangian (UL) formulation (Bathe and Bolourchi 1979, Cardona and Geradin 1988, Teh and Clarke 1999), and co-rotational (CR) formulation (Hsiao *et al*. 1987, Crisfield 1990, Felippa and Haugen 2005, Li 2007, Battini 2008).

*Corresponding author, Ph.D. Student, E-mail: LONG0026@e.ntu.edu.sg

http://www.techno-press.org/?journal=sem&subpage=8 ISSN: 1225-4568 (Print), 1598-6217 (Online)

It is challenging to simulate the coupled effects of large deformation and material failure due to the computation accuracy of strain and stress in the deformed configuration. However, based on a CR framework, all the information necessary to determine the material stress state can be derived in the local system with only pure deformation excluding the rigid-body movement. This is the most appealing advantage of CR formulations, which will result in a more accurate and efficient computational scheme on strain and stress compared with other formulations. Therefore, CR formulations are employed for the beam formulation in the present study. Nevertheless, the superiority of CR formulations was only discussed at a theoretical level (Hsiao *et al*. 1987, Felippa and Haugen 2005, Li 2007) and needs to be numerically confirmed by comparison with other formulations, such as TL formulation (Dvorkin *et al*. 1988).

There are various CR formulations (Hsiao *et al*. 1987, Crisfield 1990, Felippa and Haugen 2005, Li 2007, Battini 2008) proposed in the literature, even though they share the common characteristics in terms of CR framework. Compared to the other CR formulations, there are two main advantages of the CR formulation proposed by Li (2007). In his approach, a set of vectorial rotational variables, which are three orthogonal components of normal vectors, is defined to describe spatial rotations. Through the judicious selection of vectorial rotational variables, all variables in the incremental solution process can be treated as vectors subjected to the usual rules of commutative addition. This results in a symmetric geometric stiffness matrix both in the local and the global systems. Furthermore, updating of vectorial rotational variables in incremental loading is much simpler compared to the conventional definitions of rotational degrees of freedom using absolute rotations about coordinate axes. Thus, the general idea of the CR beam formulation by Li (2007) is advantageous over the other CR formulations.

However, this CR formulation was initially derived for linear elastic material, which is not suitable for simulating structures undergoing large deformation with material yielding and approaching failure. For material nonlinearity, there are a few publications concerning numerical and experimental aspects. There is a comprehensive review collection on material nonlinearity from Hinton and Owen (1984), but none of them can be directly applied to the CR framework by Li (2007). Therefore, if the CR beam formulation by Li (2007) were employed to predict the RC beam geometric nonlinearity, derivations for material nonlinearity at the fibre level for both steel and concrete have to be conducted in the framework of this CR formulation. This work is described in greater detail later in the present study.

In order to accurately simulate structures subjected to large deformation and material nonlinearity, the coupled effects of geometric and material nonlinearities of steel and RC structures should be incorporated for the proposed three dimensional CR beam. This is fundamental to the study of deformation behaviour of structural members at the ultimate limit state. Therefore, validations for the proposed derivations incorporating material nonlinearity will be conducted through examples including isolated steel and RC structural members, a spatial steel frame and an RC beam-column subassemblage.

In addition to the formulation derivations and material properties, computational efficiency of beam elements is also of interest when conducting finite element analysis for large-scale structures. Theoretically, CR formulations have an intrinsic advantage compared with TL and UL formulations. That is, CR formulations decompose the deformation into a rigid-body movement and a pure deformation. Moreover, the pure deformation depicted in local coordinate system is assumed to be small and can be efficiently calculated. Nevertheless, it should be pointed out that even though the CR beam formulation was proposed by Li (2007) a few years ago and since then, the efficiency advantage has been claimed, there is no direct comparison published in terms of

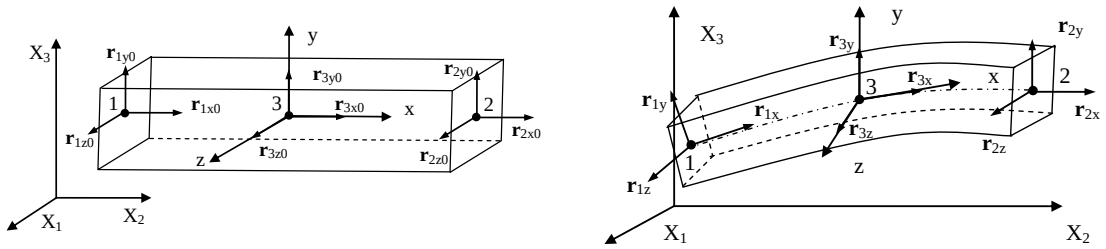

(a) The undeformed configuration of a beam (b) The deformed configuration of a beam

Fig. 1 Notation details for undeformed and deformed configurations of a CR beam

computational time. The computational efficiency has to be evaluated based on the same material model and solution technique to be absolutely fair. This requires a lot of work to be done. For example, the TL beam element proposed by Dvorkin *et al*. (1988) can be utilized to represent a typical TL formulation, and a benchmark in terms of computational accuracy and efficiency can be conducted with comparison of the CR formulation. With the main objective of this study to simulate the nonlinear behaviour of RC framed structures, the examples to conduct the benchmark tests will be based on structural problems involving geometric and material nonlinearities.

2. Co-rotational (CR) beam formulation

The greatest challenge for a 3D beam element formulation is to simulate spatial rotations. A three-node CR beam formulation is employed to simulate the geometric nonlinearity of three dimensional deformations. In the utilized CR beam formulation, rotational variables in spatial rotations are defined by vectorial rotational variables. The details of the 3D beam formulations can be found in the works by Li (2007).

Some assumptions are made the CR beam formulations. (1) In the local coordinate system the strain is small. (2) Normal vectors to the neutral axis before deformation remain straight but not necessarily normal to the neutral axis after deformation. (3) The shape of the CR beam cross-section does not warp.

The numbering sequence of a three-node CR beam is shown in Fig. 1 with the end nodes tagged as 1 and 2, and the middle node as 3. As shown in Fig. 1, both local and global coordinates systems are created in order to describe the local and global displacements and rotations. The local system {x, y, z} remains fixed with the middle node (Node 3) and does not deform with the movement of the element. The local x axis is set to be tangential to the beam longitudinal axis by default. Therefore, there are only two active end nodes (Nodes 1 and 2) for the CR beam element in the local coordinate system. Directional changes of the local *y* and *z* axes imply the local deformation of the beam element. The degrees of freedom in the local and global systems are

$$\mathbf{u}_L = \left\{ u_1 \; v_1 \; w_1 \; r_{1y,n_1} \; r_{1y,m_1} \; r_{1z,n_1} \; u_2 \; v_2 \; w_2 \; r_{2y,n_2} \; r_{2y,m_2} \; r_{2z,n_2} \right\}^{\mathrm{T}}$$

and $$\mathbf{u}_G = \left\{ U_1 \; V_1 \; W_1 \; e_{1y,n_1} \; e_{1y,m_1} \; e_{1z,n_1} \; U_2 \; V_2 \; W_2 \; e_{2y,n_2} \; e_{2y,m_2} \; e_{2z,n_2} \; U_3 \; V_3 \; W_3 \; e_{3y,n_3} \; e_{3y,m_3} \; e_{3z,n_3} \right\}^{\mathrm{T}}$$

where u_i, v_i, w_i are the local displacements of Node i (i=1,2), r_{iy,n_i}, r_{iy,m_i}, r_{iz,n_i} are the *local* vectorial rotational variables representing the rotation of Node i (i=1,2). The terms U_i, V_i, W_i are the global displacements of Node i (i=1,2,3) and e_{iy,n_i}, e_{iy,m_i}, e_{iz,n_i} are the *global* vectorial rotational variables representing the rotation of Node i (i=1,2,3). The subscripts n_i and m_i indicate the nth and mth components of the direction vectors of Node i. The vectorial rotational variables r_{iy,n_i}, r_{iy,m_i}, r_{iz,n_i} in the local coordinate system and e_{iy,n_i}, e_{iy,m_i}, e_{iz,n_i} in the global coordinate system are, respectively, defined according to the relative quantities and permutation sequence of all three components for direction vectors $\mathbf{r}_{iy}$ and $\mathbf{r}_{iz}$ of Node i in the local system (see Fig. 1) and direction vectors $\mathbf{e}_{iy}$ and $\mathbf{e}_{iz}$ of Node i in the global system as discussed by Li (2007). For example, assuming $|r_{iy,l_i}| > |r_{iy,n_i}|$ and $|r_{iy,l_i}| > |r_{iy,m_i}|$ ($n,m,l \in \{1,2,3\}$ and $n \neq m \neq l$), if $|r_{iz,l_i}| > |r_{iz,n_i}|$ and $|r_{iz,l_i}| > |r_{iz,m_i}|$ are satisfied, then the values of n , m and l follow a cyclic permutation of {1,2,3}. In the case of a beam bending slightly in the local x-y plane, the direction vectors $\mathbf{r}_{1y}$ and $\mathbf{r}_{2y}$ at Nodes 1 and 2 slightly rotate about the local z axis, then the component with the maximum value among all three components should be the one along the local y axis, that is, l should be equal to 2 with n equal to 3 and m equal to 1. After each load increment or iteration, the vectorial rotational variables should be updated based on the orthogonality conditions $\mathbf{r}_{iy}^{\mathrm{T}}\mathbf{r}_{iz}=0$ and $\mathbf{e}_{iy}^{\mathrm{T}}\mathbf{e}_{iz}=0$.

In addition, the definition of the local system {x, y, z} as shown in Fig. 1 indicates the cross-sectional orientation of the CR beam element. The direction of local y axis is taken as the weak axis direction, whereas local z axis is the stronger axis direction. Both the local system {x, y, z} and the global system {X_1, X_2, X_3} follow the right-hand rule.

Since the CR formulation decomposes the incremental deformations into a rigid-body movement and pure deformations, the deformations in the local coordinate system is assumed to be small. The deformation at any point of the element can be obtained based on nodal deformations by means of quadratic Lagrangian interpolation functions.

$$\mathbf{u} = \sum_{i=1}^{3} h_i(\zeta)\left[\mathbf{t}_i + y\left(\mathbf{r}_{iy} - \mathbf{r}_{iy0}\right) + z\left(\mathbf{r}_{iz} - \mathbf{r}_{iz0}\right)\right] \tag{1}$$

where $\mathbf{t}_i=\{u_i,\ v_i,\ w_i\}^{\mathrm{T}}$ consists of the local nodal translational displacements; $\mathbf{r}_{iy0}$ and $\mathbf{r}_{iy}$ are direction vectors along the cross-sectional weak axis (local y axis) at Node i before and after deformation, respectively (see Fig. 1); $\mathbf{r}_{iz0}$ and $\mathbf{r}_{iz}$ are direction vectors along the cross-sectional strong axis (local z axis) at Node i before and after deformation, respectively (see Fig. 1); y and z are the local coordinates along the cross-sectional weak and strong axes of the beam element; h_i is the Lagrangian interpolation function; ζ is one-dimensional natural coordinate along the centre line of the beam element.

As the first derivative of displacement with respect to local degrees of freedom $\mathbf{u}_L$, the corresponding strain in the local coordinate system is based on Green strain. In a compact form (Li 2007), Green strain can be written as

$$\boldsymbol{\varepsilon} = \boldsymbol{\varepsilon}^{(0)} + y\boldsymbol{\varepsilon}^{(1)} + z\boldsymbol{\varepsilon}^{(2)} + yz\boldsymbol{\varepsilon}^{(3)} + y^2\boldsymbol{\varepsilon}^{(4)} + z^2\boldsymbol{\varepsilon}^{(5)} \tag{2}$$

The six coefficients of $\boldsymbol{\varepsilon}$ are derived by the author of this paper and are listed below for completeness.

$$\boldsymbol{\varepsilon}^{(0)}=\begin{Bmatrix}\frac{1}{2}\frac{\partial \mathbf{u}_t}{\partial x}\frac{\partial \mathbf{u}_t}{\partial x}+\frac{\partial \mathbf{u}_t}{\partial x}\frac{\partial \mathbf{x}_0}{\partial x}\\ \frac{\partial \mathbf{u}_t}{\partial x}\mathbf{r}_y+\frac{\partial \mathbf{x}_0}{\partial x}(\mathbf{r}_y-\mathbf{r}_{y0})\\ \frac{\partial \mathbf{u}_t}{\partial x}\mathbf{r}_z+\frac{\partial \mathbf{x}_0}{\partial x}(\mathbf{r}_z-\mathbf{r}_{z0})\end{Bmatrix}\quad \boldsymbol{\varepsilon}^{(1)}=\begin{Bmatrix}\frac{\partial \mathbf{u}_t}{\partial x}\frac{\partial \mathbf{r}_y}{\partial x}+\frac{\partial \mathbf{x}_0}{\partial x}\frac{\partial(\mathbf{r}_y-\mathbf{r}_{y0})}{\partial x}\\ \frac{\partial \mathbf{r}_y}{\partial x}\mathbf{r}_y-\frac{\partial \mathbf{r}_{y0}}{\partial x}\mathbf{r}_{y0}\\ \frac{\partial \mathbf{r}_y}{\partial x}\mathbf{r}_z-\frac{\partial \mathbf{r}_{y0}}{\partial x}\mathbf{r}_{z0}\end{Bmatrix}\quad \boldsymbol{\varepsilon}^{(2)}=\begin{Bmatrix}\frac{\partial \mathbf{u}_t}{\partial x}\frac{\partial \mathbf{r}_z}{\partial x}+\frac{\partial \mathbf{x}_0}{\partial x}\frac{\partial(\mathbf{r}_z-\mathbf{r}_{z0})}{\partial x}\\ \frac{\partial \mathbf{r}_z}{\partial x}\mathbf{r}_y-\frac{\partial \mathbf{r}_{z0}}{\partial x}\mathbf{r}_{y0}\\ \frac{\partial \mathbf{r}_z}{\partial x}\mathbf{r}_z-\frac{\partial \mathbf{r}_{z0}}{\partial x}\mathbf{r}_{z0}\end{Bmatrix}$$

$$\boldsymbol{\varepsilon}^{(3)}=\begin{Bmatrix}\frac{\partial \mathbf{r}_y}{\partial x}\frac{\partial \mathbf{r}_z}{\partial x}-\frac{\partial \mathbf{r}_{y0}}{\partial x}\frac{\partial \mathbf{r}_{z0}}{\partial x}\\ 0\\ 0\end{Bmatrix}\quad \boldsymbol{\varepsilon}^{(4)}=\begin{Bmatrix}\frac{1}{2}\left(\frac{\partial \mathbf{r}_y}{\partial x}\frac{\partial \mathbf{r}_y}{\partial x}-\frac{\partial \mathbf{r}_{y0}}{\partial x}\frac{\partial \mathbf{r}_{y0}}{\partial x}\right)\\ 0\\ 0\end{Bmatrix}\quad \boldsymbol{\varepsilon}^{(5)}=\begin{Bmatrix}\frac{1}{2}\left(\frac{\partial \mathbf{r}_z}{\partial x}\frac{\partial \mathbf{r}_z}{\partial x}-\frac{\partial \mathbf{r}_{z0}}{\partial x}\frac{\partial \mathbf{r}_{z0}}{\partial x}\right)\\ 0\\ 0\end{Bmatrix}$$

where $\mathbf{x}_0=\{x_0, y_0, z_0\}^{\mathrm{T}}$ is the local coordinate at any point in the beam element; $\mathbf{r}_{y0}=\sum_{i=1}^{3}h_i(\zeta)\mathbf{r}_{iy0}$ is the initial direction vector along the cross-sectional weak axis at any point; $\mathbf{r}_y=\sum_{i=1}^{3}h_i(\zeta)\mathbf{r}_{iy}$ is the current direction vector along the cross-sectional weak axis at any point after deformation; $\mathbf{r}_{z0}=\sum_{i=1}^{3}h_i(\zeta)\mathbf{r}_{iz0}$ is the initial direction vector along the cross-sectional strong axis at any point; $\mathbf{r}_z=\sum_{i=1}^{3}h_i(\zeta)\mathbf{r}_{iz}$ is the current direction vector along the cross-sectional strong axis at any point after deformation; $\mathbf{u}_t=\sum_{i=1}^{3}h_i(\zeta)\mathbf{t}_i$ is the translational displacements at any point. The subscript *i* indicates the corresponding function at node *i*; the subscript 0 indicates the function in the state *before deformation* and if there is no 0, the function is in the *current deformed state* as shown in Fig. 1. Jacobian matrix is calculated as the relationship between the natural coordinate system and the local coordinate system.

With respect to the local unknown variables $\mathbf{u}_L$, the geometric matrix **B** can be expressed in a compact form as

$$\begin{aligned}\mathbf{B}&=\frac{\partial \boldsymbol{\varepsilon}}{\partial \mathbf{u}_L}=\frac{\partial \boldsymbol{\varepsilon}^{(0)}}{\partial \mathbf{u}_L}+y_l\frac{\partial \boldsymbol{\varepsilon}^{(1)}}{\partial \mathbf{u}_L}+z_l\frac{\partial \boldsymbol{\varepsilon}^{(2)}}{\partial \mathbf{u}_L}+y_lz_l\frac{\partial \boldsymbol{\varepsilon}^{(3)}}{\partial \mathbf{u}_L}+{y_l}^2\frac{\partial \boldsymbol{\varepsilon}^{(4)}}{\partial \mathbf{u}_L}+{z_l}^2\frac{\partial \boldsymbol{\varepsilon}^{(5)}}{\partial \mathbf{u}_L}\\ &=\mathbf{B}^{(0)}+y_l\mathbf{B}^{(1)}+z_l\mathbf{B}^{(2)}+y_lz_l\mathbf{B}^{(3)}+{y_l}^2\mathbf{B}^{(4)}+{z_l}^2\mathbf{B}^{(5)}\end{aligned}$$

where **B** is a 3×12 matrix relating element strains and local displacements.

With the definition of Green Strain **ε** and geometric matrix **B**, it is straightforward to obtain the expression of internal force vector $\mathbf{f}_L$ and stiffness matrix $\mathbf{K}_L$ in the local coordinate system for CR beam. The strain energy of the CR beam element can be expressed as

$$U=\int_V\frac{1}{2}\boldsymbol{\varepsilon}^{\mathrm{T}}\mathbf{D}\boldsymbol{\varepsilon}\,dV\quad \text{where}\quad \mathbf{D}=\begin{bmatrix}E & 0 & 0\\ 0 & k_0G & 0\\ 0 & 0 & k_0G\end{bmatrix}\tag{3}$$

where **D** is the elastic matrix to represent the material property; *E* and *G* are the elastic modulus and shear modulus, respectively; k_0 is the shear factor depending on the shape of the employed

cross-section and is equal to 5/6 for a rectangular cross-section; V is the volume of a CR beam element.

The first derivative of strain energy with respect to unknown variables $\mathbf{u}_L$ in the local coordinate system leads to local internal force vector $\mathbf{f}_L$.

$$\mathbf{f}_L = \frac{\partial U}{\partial \mathbf{u}_L} = \int_V \frac{1}{2} \frac{\partial \boldsymbol{\varepsilon}^{\mathrm{T}}}{\partial \mathbf{u}_L} \mathbf{D}\boldsymbol{\varepsilon}\, dV + \int_V \frac{1}{2} \boldsymbol{\varepsilon}^{\mathrm{T}} \mathbf{D} \frac{\partial \boldsymbol{\varepsilon}}{\partial \mathbf{u}_L}\, dV = \int_V \mathbf{B}^{\mathrm{T}} \mathbf{D}\boldsymbol{\varepsilon}\, dV \tag{4}$$

The first derivative of out-of-balance force (internal force $\mathbf{f}_L$ minus external load $\mathbf{P}$) with respect to local unknown variables can be used to calculate the local stiffness matrix $\mathbf{K}_L$.

$$\begin{aligned} \mathbf{K}_L &= \frac{\partial (\mathbf{f}_L - \mathbf{P})}{\partial \mathbf{u}_L} = \frac{\partial}{\partial \mathbf{u}_L} \left[\int_V \mathbf{B}^{\mathrm{T}} \mathbf{D}\boldsymbol{\varepsilon}\, dV \right] \\ &= \int_V \mathbf{B}^{\mathrm{T}} \mathbf{D}\mathbf{B}\, dV + \int_V \boldsymbol{\varepsilon}^{\mathrm{T}} \mathbf{D} \frac{\partial \mathbf{B}}{\partial \mathbf{u}_L}\, dV \end{aligned} \tag{5}$$

Substituting the compact form of Green strain and geometric matrix into the local internal force vector $\mathbf{f}_L$, Eq. (4) can be rewritten as

$$\begin{aligned} \mathbf{f}_L &= \int_V \mathbf{B}^{\mathrm{T}} \mathbf{D}\boldsymbol{\varepsilon}\, dV = \int_L \int_A \left[\mathbf{B}^{\mathrm{T}} \mathbf{D}\boldsymbol{\varepsilon} \right] dA dx \\ &= \int_L \int_A \Big\{ \left[\mathbf{B}^{(0)} + y_l \mathbf{B}^{(1)} + z_l \mathbf{B}^{(2)} + y_l z_l \mathbf{B}^{(3)} + y_l{}^2 \mathbf{B}^{(4)} + z_l{}^2 \mathbf{B}^{(5)} \right]^{\mathrm{T}} \cdot \\ &\quad \mathbf{D} \left[\boldsymbol{\varepsilon}^{(0)} + y_l \boldsymbol{\varepsilon}^{(1)} + z_l \boldsymbol{\varepsilon}^{(2)} + y_l z_l \boldsymbol{\varepsilon}^{(3)} + y_l{}^2 \boldsymbol{\varepsilon}^{(4)} + z_l{}^2 \boldsymbol{\varepsilon}^{(5)} \right] \Big\} dA dx \end{aligned} \tag{6}$$

where the scalar terms A and L are the cross-sectional area and the length of CR beam, respectively.

When incorporating the fibre model into the CR beam formulation, for the convenience of programming, local internal force vector $\mathbf{f}_L$ can also be rewritten in the form of Eq. (7) by expanding Eq. (6).

$$\mathbf{f}_L = \int_L \left[\sum_{i=1}^{14} C_i \mathbf{f}_i \right] dx \tag{7}$$

where the coefficients C_i (i=1,…,14) are derived as follows.

$C_0 = \int_A dA$, $C_1 = \int_A y_l dA$, $C_2 = \int_A z_l dA$, $C_3 = \int_A y_l z_l dA$, $C_4 = \int_A y_l^2 dA$, $C_5 = \int_A z_l^2 dA$,
$C_6 = \int_A y_l^2 z_l dA$, $C_7 = \int_A y_l z_l^2 dA$, $C_8 = \int_A y_l^2 z_l^2 dA$, $C_9 = \int_A y_l^4 dA$, $C_{10} = \int_A z_l^4 dA$, $C_{11} = \int_A y_l^3 dA$,
$C_{12} = \int_A z_l^3 dA$, $C_{13} = \int_A y_l^3 z_l dA$, $C_{14} = \int_A y_l z_l^3 dA$.

Details of the vectors $\mathbf{f}_i$ (i=1,…,14) can be found in Appendix A. Similarly, after substituting the Green strain and geometric matrix into the local stiffness matrix $\mathbf{K}_L$, the tangential stiffness matrix in the local coordinate system can be written as

$$\begin{aligned}\mathbf{K}_L &= \int_V \mathbf{B}^{\mathrm{T}}\mathbf{D}\mathbf{B}\, dV + \int_V \boldsymbol{\varepsilon}^{\mathrm{T}}\mathbf{D}\frac{\partial \mathbf{B}}{\partial \mathbf{u}_L}\, dV = \int_L \int_A \left[\mathbf{B}^{\mathrm{T}}\mathbf{D}\mathbf{B} + \boldsymbol{\varepsilon}^{\mathrm{T}}\mathbf{D}\frac{\partial \mathbf{B}}{\partial \mathbf{u}_L} \right] dA dx \\ &= \int_L \int_A \Big\{ \left[\mathbf{B}^{(0)} + y_l\mathbf{B}^{(1)} + z_l\mathbf{B}^{(2)} + y_l z_l \mathbf{B}^{(3)} + {y_l}^2\mathbf{B}^{(4)} + {z_l}^2\mathbf{B}^{(5)} \right]^{\mathrm{T}} \\ &\quad \mathbf{D}\left[\mathbf{B}^{(0)} + y_l\mathbf{B}^{(1)} + z_l\mathbf{B}^{(2)} + y_l z_l \mathbf{B}^{(3)} + {y_l}^2\mathbf{B}^{(4)} + {z_l}^2\mathbf{B}^{(5)} \right] \\ &\quad + \left[\boldsymbol{\varepsilon}^{(0)} + y_l\boldsymbol{\varepsilon}^{(1)} + z_l\boldsymbol{\varepsilon}^{(2)} + y_l z_l \boldsymbol{\varepsilon}^{(3)} + {y_l}^2\boldsymbol{\varepsilon}^{(4)} + {z_l}^2\boldsymbol{\varepsilon}^{(5)} \right]^{\mathrm{T}} \\ &\quad \mathbf{D}\left[\frac{\partial \mathbf{B}^{(0)}}{\partial \mathbf{u}_L} + y_l \frac{\partial \mathbf{B}^{(1)}}{\partial \mathbf{u}_L} + z_l \frac{\partial \mathbf{B}^{(2)}}{\partial \mathbf{u}_L} + y_l z_l \frac{\partial \mathbf{B}^{(3)}}{\partial \mathbf{u}_L} + {y_l}^2 \frac{\partial \mathbf{B}^{(4)}}{\partial \mathbf{u}_L} + {z_l}^2 \frac{\partial \mathbf{B}^{(5)}}{\partial \mathbf{u}_L} \right] \Big\} dA dx \end{aligned} \tag{8}$$

The tangential stiffness matrix can also be expressed in the form of Eq. (9) by expanding Eq. (8).

$$\mathbf{K}_L = \int_L \left[\sum_{i=1}^{14} C_i \mathbf{K}_i \right] dx \tag{9}$$

where the coefficients C_i are the same as those in Eq. (7) and the details of the sub-matrices $\mathbf{K}_i$ (i=1,…,14) are given in Appendix B. These are derived by the author of this paper. According to the transformation matrix $\mathbf{T}$ from the local to the global coordinate system form (Li 2007), global internal force vector $\mathbf{f}_G$ and tangential stiffness matrix $\mathbf{K}_G$ can be derived, respectively.

$$\mathbf{f}_G = \mathbf{T}^{\mathrm{T}}\mathbf{f}_L \quad \text{and} \quad \mathbf{K}_G = \mathbf{T}^{\mathrm{T}}\mathbf{K}_L\mathbf{T} + \frac{\partial \mathbf{T}^{\mathrm{T}}}{\partial \mathbf{u}_G}\mathbf{f}_L \tag{10}$$

It should be noted that the derivations of local internal force vector and stiffness matrix are for general beam cross-sections including non-symmetric sections, so that non-symmetric steel reinforcement for a concrete beam section can be modelled and this will be discussed next.

3. Fibre model

After the internal force vector $\mathbf{f}_L$ and stiffness matrix $\mathbf{K}_L$ in the local coordinate for the CR beam have been computed from Eq. (6) and Eq. (8), they can be expressed in the form of

$$\mathbf{f}_L = \int_L \int_A \left[\mathbf{B}^{\mathrm{T}}\mathbf{D}\boldsymbol{\varepsilon} \right] dA dx \quad \text{and} \quad \mathbf{K}_L = \int_L \int_A \left[\mathbf{B}^{\mathrm{T}}\mathbf{D}\mathbf{B} + \boldsymbol{\varepsilon}^{\mathrm{T}}\mathbf{D}\frac{\partial \mathbf{B}}{\partial \mathbf{u}_L} \right] dA dx \tag{11}$$

Conventionally, in the process of three dimensional integration, both the local internal force vector $\mathbf{f}_L$ and local stiffness matrix $\mathbf{K}_L$ can be obtained by integrating certain functions at the cross-section A and then integrating them along the element length L. That is, the integration can be treated as an integration of a known function $\mathbf{X}$ with respect to the cross-section A and element length L to obtain $\mathbf{F}$, as expressed in Eq. (12).

$$\mathbf{F} = \int_L \int_A [\mathbf{X}] dA dx \tag{12}$$

Since the integration of **X** can be performed at the cross-section of each fibre first and then summed up together to obtain the integrated value around the entire cross-section, the material properties and the cross-sectional shape can be implemented at the fibre level. The cross-section may contain fibres with different material properties (or even voids) or different shapes. Fig. 2(a) shows a non-symmetric section. However, the assumption of "plane sections remain plane" has to be kept, so that the studied beam element is assumed to be laterally restrained and no warping effect is considered.

To simulate RC members, steel reinforcement and concrete are assigned to different fibres. Fibre model assumes perfect bond between concrete and reinforcement. Therefore, the integration process provides the opportunity to employ fibre model to represent the CR beam cross-section and to simulate more accurately the mechanical behaviour and the stress and strain constitutive relations at specified 'cells" around the CR beam cross-sections. By employing the fibre model, the local internal force vector $\mathbf{f}_L$ and local stiffness matrix $\mathbf{K}_L$ can be expressed as

$$\mathbf{f}_L = \int_L \sum_{NF} \left[\sum_{i=1}^{14} C_i \mathbf{f}_i \right] dx \quad \text{and} \quad \mathbf{K}_L = \int_L \sum_{NF} \left[\sum_{i=1}^{14} C_i \mathbf{K}_i \right] dx \qquad (13)$$

where *NF* is the number of fibres of the cross-section at the Gaussian point along the longitudinal axis of the CR beam element (Fig. 2 (b)); the coefficients C_i (i=1,…,14) at the fibre cross-sections are first computed by using Eq. (7) and $\sum_{i=1}^{14} C_i \mathbf{f}_i$ at the fibre level can be computed conveniently. The summation of $\sum_{i=1}^{14} C_i \mathbf{f}_i$ from all of the fibres, which is the integrated value for the whole cross-sectional area at a Gaussian point along a CR beam element, can then be obtained. The calculation procedure of local stiffness matrix $\mathbf{K}_L$ follows the same way.

It should be noted that reduced integration with two Gaussian points along the longitudinal axis of the proposed three-node CR beam element is adopted as explicitly described in Fig. 2(b). However, a lower order integration scheme (i.e. single-point integration) for each fibre around the cross-section is utilized with the assumption of uniform stress for each fibre area. In all of the examples employed in the present paper, single-point integration is applied for fibre model by default.

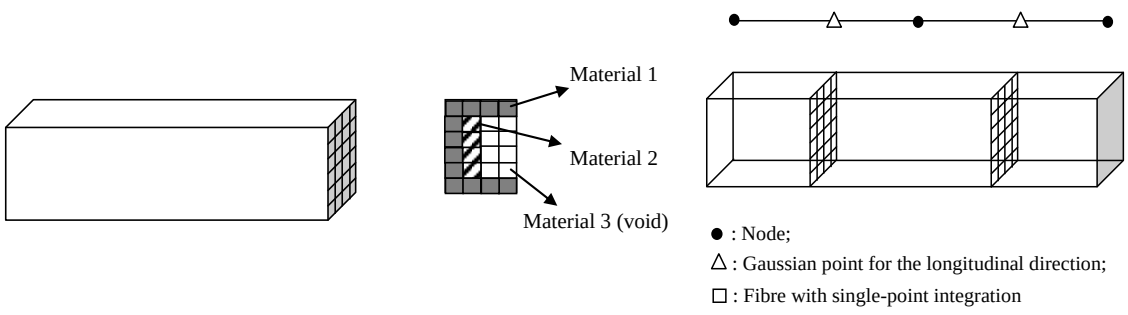

(a) Distribution of fibres with different material properties

(b) Fibre model and integration procedure for a CR beam

Fig. 2 Fibre model of a CR beam

4. Material nonlinearity

When handling material nonlinearity for RC structures, steel reinforcement is treated as an elasto-plastic material with Von Mises yield criterion which conforms to associated flow rule, plastic potential and normality condition. On the other hand, the constitutive relationship of concrete is assumed to follow empirical formulae (Karsan and Jirsa 1969, Rots *et al*. 1984, Barzegar-Jamshidi 1987, Dvorkin *et al*. 1988, Taucer *et al*. 1991) which have been widely employed and verified to be suitable for numerical computation.

4.1 Steel reinforcement

From Hinton and Owen (1984), the elasto-plastic incremental stress-strain relation is given as

$$d\boldsymbol{\sigma} = \mathbf{D}_{ep} d\boldsymbol{\varepsilon} \tag{14}$$

where the equivalent material matrix $\mathbf{D}_{ep}=\mathbf{D}-\mathbf{D}\mathbf{a}\mathbf{a}^{\mathrm{T}}\mathbf{D}/(H+\mathbf{a}^{\mathrm{T}}\mathbf{D}\mathbf{a})$, $\mathbf{D}$ is the elastic material matrix, flow vector $\mathbf{a}=\partial F/\partial\boldsymbol{\sigma}$ and F is the yield function indicating the plastic state of the material in yield criteria. Therefore

$$d\boldsymbol{\sigma} = \mathbf{D}_{ep} d\boldsymbol{\varepsilon} = \mathbf{D}d\boldsymbol{\varepsilon} - \frac{\mathbf{D}\mathbf{a}\mathbf{a}^{\mathrm{T}}\mathbf{D}}{H+\mathbf{a}^{\mathrm{T}}\mathbf{D}\mathbf{a}} d\boldsymbol{\varepsilon} = d\boldsymbol{\sigma}_e - \mathbf{D}\mathbf{a}\frac{\mathbf{a}^{\mathrm{T}}\mathbf{D}d\boldsymbol{\varepsilon}}{H+\mathbf{a}^{\mathrm{T}}\mathbf{D}\mathbf{a}} = d\boldsymbol{\sigma}_e - d\lambda\mathbf{D}\mathbf{a} \tag{15}$$

where $d\lambda=\mathbf{a}^{\mathrm{T}}\mathbf{D}d\boldsymbol{\varepsilon}/(H+\mathbf{a}^{\mathrm{T}}\mathbf{D}\mathbf{a})$.

With a common procedure to handle problems including elasto-plastic and strain hardening behaviour, the stress increments can be divided into one part inside the yield surface and another part outside the yield surface, with R as the ratio of the part outside the yield surface to the whole stress increment, as shown in detail in Fig. 3.

$$d\boldsymbol{\sigma}_e = (1-R)d\boldsymbol{\sigma}_e + Rd\boldsymbol{\sigma}_e \tag{16}$$

Substituting the part outside the yield surface $Rd\boldsymbol{\sigma}_e$ back to the elasto-plastic incremental stress-strain relation $d\boldsymbol{\sigma}=d\boldsymbol{\sigma}_e-d\lambda\mathbf{D}\mathbf{a}$ and considering the contribution from the part inside the yield surface, the whole incremental stress can be obtained as

$$d\boldsymbol{\sigma} = (1-R)d\boldsymbol{\sigma}_e + Rd\boldsymbol{\sigma}_e - d\lambda\mathbf{D}\mathbf{a} \tag{17}$$

where $d\lambda=\mathbf{a}^{\mathrm{T}}\mathbf{D}Rd\boldsymbol{\varepsilon}/(H+\mathbf{a}^{\mathrm{T}}\mathbf{D}\mathbf{a})$.

The plastic part outside the yield surface $Rd\boldsymbol{\sigma}_e-d\lambda\mathbf{D}\mathbf{a}$ will be eliminated through several iterations. After that, the elasto-plastic incremental stress-strain relation for the first iteration can be expressed as

$$d\boldsymbol{\sigma} = (1-R)d\boldsymbol{\sigma}_e + \frac{Rd\boldsymbol{\sigma}_e}{m} - \frac{d\lambda\mathbf{D}\mathbf{a}}{m} \tag{18}$$

where m is the user-defined iteration number and is suggested to be the nearest integer which is less than $8(Rd\boldsymbol{\sigma}_e/\boldsymbol{\sigma}_{Y0})+1$, where $\boldsymbol{\sigma}_{Y0}$ is the initial uniaxial yield strength.

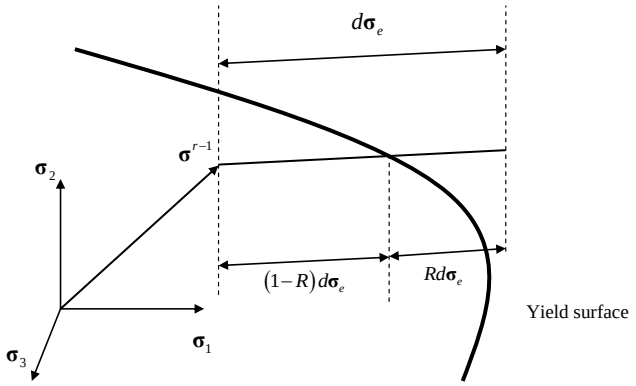

Fig. 3 Incremental stress changes in an elasto-plastic material

In the present CR beam formulation, the strain is calculated in the form

$$\boldsymbol{\varepsilon} = \boldsymbol{\varepsilon}^{(0)} + y_l\boldsymbol{\varepsilon}^{(1)} + z_l\boldsymbol{\varepsilon}^{(2)} + y_l z_l\boldsymbol{\varepsilon}^{(3)} + {y_l}^2\boldsymbol{\varepsilon}^{(4)} + {z_l}^2\boldsymbol{\varepsilon}^{(5)} \tag{19}$$

The incremental strain can be then written in the form

$$d\boldsymbol{\varepsilon} = d\boldsymbol{\varepsilon}^{(0)} + y_l d\boldsymbol{\varepsilon}^{(1)} + z_l d\boldsymbol{\varepsilon}^{(2)} + y_l z_l d\boldsymbol{\varepsilon}^{(3)} + {y_l}^2 d\boldsymbol{\varepsilon}^{(4)} + {z_l}^2 d\boldsymbol{\varepsilon}^{(5)} \tag{20}$$

So the incremental stress is given as

$$\begin{aligned} d\boldsymbol{\sigma} &= (1-R)\mathbf{D}d\boldsymbol{\varepsilon} + \frac{R\mathbf{D}d\boldsymbol{\varepsilon}}{m} - \frac{1}{m}\left(\frac{\mathbf{a}^{\mathrm{T}}\mathbf{D}Rd\boldsymbol{\varepsilon}}{H+\mathbf{a}^{\mathrm{T}}\mathbf{D}\mathbf{a}}\right)\mathbf{D}\mathbf{a} \\ &= \left[(1-R)\mathbf{D} + \frac{R\mathbf{D}}{m}\right]d\boldsymbol{\varepsilon} - \frac{1}{m}\left(\frac{\mathbf{a}^{\mathrm{T}}\mathbf{D}}{H+\mathbf{a}^{\mathrm{T}}\mathbf{D}\mathbf{a}}\cdot Rd\boldsymbol{\varepsilon}\right)\mathbf{D}\mathbf{a} \end{aligned}$$

$$\begin{aligned} &= \left[(1-R)\mathbf{D} + \frac{R\mathbf{D}}{m}\right]\left(d\boldsymbol{\varepsilon}^{(0)} + y_l d\boldsymbol{\varepsilon}^{(1)} + z_l d\boldsymbol{\varepsilon}^{(2)} + y_l z_l d\boldsymbol{\varepsilon}^{(3)} + {y_l}^2 d\boldsymbol{\varepsilon}^{(4)} + {z_l}^2 d\boldsymbol{\varepsilon}^{(5)}\right) \\ &\quad - \frac{1}{m}\left[\frac{\mathbf{a}^{\mathrm{T}}\mathbf{D}}{H+\mathbf{a}^{\mathrm{T}}\mathbf{D}\mathbf{a}}\cdot R\left(d\boldsymbol{\varepsilon}^{(0)} + y_l d\boldsymbol{\varepsilon}^{(1)} + z_l d\boldsymbol{\varepsilon}^{(2)} + y_l z_l d\boldsymbol{\varepsilon}^{(3)} + {y_l}^2 d\boldsymbol{\varepsilon}^{(4)} + {z_l}^2 d\boldsymbol{\varepsilon}^{(5)}\right)\right]\mathbf{D}\mathbf{a} \end{aligned} \tag{21}$$

In general, assuming that vector $\mathbf{x}$ can be expressed as $\alpha_1\mathbf{x}_1 + \alpha_2\mathbf{x}_2$ where α_1 and α_2 are scalar quantities, the matrix-vector computation can be performed as follows.

$$(\mathbf{a}\cdot\mathbf{x})\mathbf{c} = \left[\mathbf{a}\cdot(\alpha_1\mathbf{x}_1 + \alpha_2\mathbf{x}_2)\right]\mathbf{c} = (\mathbf{a}\cdot\alpha_1\mathbf{x}_1)\mathbf{c} + (\mathbf{a}\cdot\alpha_2\mathbf{x}_2)\mathbf{c} = \alpha_1(\mathbf{a}\cdot\mathbf{x}_1)\mathbf{c} + \alpha_2(\mathbf{a}\cdot\mathbf{x}_2)\mathbf{c} \tag{22}$$

From Eq. (22), the expression $(\mathbf{a}\cdot\mathbf{x})\mathbf{c}$ can be calculated by superposition of vector components. So the incremental stress in Eq. (21) can be rewritten as

$$
\begin{aligned}
d\boldsymbol{\sigma} = & \left[\left(1-R\right)\mathbf{D} + \frac{R\mathbf{D}}{m} \right] \left(d\boldsymbol{\varepsilon}^{(0)} + y_l d\boldsymbol{\varepsilon}^{(1)} + z_l d\boldsymbol{\varepsilon}^{(2)} + y_l z_l d\boldsymbol{\varepsilon}^{(3)} + {y_l}^2 d\boldsymbol{\varepsilon}^{(4)} + {z_l}^2 d\boldsymbol{\varepsilon}^{(5)} \right) \\
& - \frac{1}{m} \left[\frac{\mathbf{a}^{\mathrm{T}}\mathbf{D}}{H + \mathbf{a}^{\mathrm{T}}\mathbf{D}\mathbf{a}} \cdot R d\boldsymbol{\varepsilon}^{(0)} \right] \mathbf{D}\mathbf{a} - y_l \frac{1}{m} \left[\frac{\mathbf{a}^{\mathrm{T}}\mathbf{D}}{H + \mathbf{a}^{\mathrm{T}}\mathbf{D}\mathbf{a}} \cdot R d\boldsymbol{\varepsilon}^{(1)} \right] \mathbf{D}\mathbf{a} \\
& - z_l \frac{1}{m} \left[\frac{\mathbf{a}^{\mathrm{T}}\mathbf{D}}{H + \mathbf{a}^{\mathrm{T}}\mathbf{D}\mathbf{a}} \cdot R d\boldsymbol{\varepsilon}^{(2)} \right] \mathbf{D}\mathbf{a} - y_l z_l \frac{1}{m} \left[\frac{\mathbf{a}^{\mathrm{T}}\mathbf{D}}{H + \mathbf{a}^{\mathrm{T}}\mathbf{D}\mathbf{a}} \cdot R d\boldsymbol{\varepsilon}^{(3)} \right] \mathbf{D}\mathbf{a} \\
& - {y_l}^2 \frac{1}{m} \left[\frac{\mathbf{a}^{\mathrm{T}}\mathbf{D}}{H + \mathbf{a}^{\mathrm{T}}\mathbf{D}\mathbf{a}} \cdot R d\boldsymbol{\varepsilon}^{(4)} \right] \mathbf{D}\mathbf{a} - {z_l}^2 \frac{1}{m} \left[\frac{\mathbf{a}^{\mathrm{T}}\mathbf{D}}{H + \mathbf{a}^{\mathrm{T}}\mathbf{D}\mathbf{a}} \cdot R d\boldsymbol{\varepsilon}^{(5)} \right] \mathbf{D}\mathbf{a}
\end{aligned} \tag{23}
$$

Defining the term $d\lambda_i$ as follows

$$
d\lambda_i = \frac{1}{m} \frac{\mathbf{a}^{\mathrm{T}}\mathbf{D}}{H + \mathbf{a}^{\mathrm{T}}\mathbf{D}\mathbf{a}} \cdot R d\boldsymbol{\varepsilon}^{(i)}, \quad i = 0, 1, \ldots, 5 \tag{24}
$$

the incremental stress and the components cast in the CR framework can be specified as

$$
d\boldsymbol{\sigma} = d\boldsymbol{\sigma}^{(0)} + y_l d\boldsymbol{\sigma}^{(1)} + z_l d\boldsymbol{\sigma}^{(2)} + y_l z_l d\boldsymbol{\sigma}^{(3)} + {y_l}^2 d\boldsymbol{\sigma}^{(4)} + {z_l}^2 d\boldsymbol{\sigma}^{(5)} \tag{25}
$$

where

$$
d\boldsymbol{\sigma}^{(i)} = \left(1-R\right)\mathbf{D} d\boldsymbol{\varepsilon}^{(i)} + \frac{R\mathbf{D}}{m} d\boldsymbol{\varepsilon}^{(i)} - d\lambda_i \mathbf{D}\mathbf{a}
$$

and

$$
d\lambda_i = \frac{1}{m} \frac{\mathbf{a}^{\mathrm{T}}\mathbf{D}}{H + \mathbf{a}^{\mathrm{T}}\mathbf{D}\mathbf{a}} \cdot R d\boldsymbol{\varepsilon}^{(i)}, \quad i = 0, 1, \ldots, 5.
$$

4.2 Concrete

Similarly, the elasto-plastic incremental stress-strain relation for concrete materials is also written in the form of

$$
d\boldsymbol{\sigma} = \mathbf{D}_{ep} d\boldsymbol{\varepsilon} \qquad \text{where} \quad \mathbf{D}_{ep} = \begin{bmatrix} E & 0 & 0 \\ 0 & k_0 G & 0 \\ 0 & 0 & k_0 G \end{bmatrix} \tag{26}
$$

where $\mathbf{D}_{ep}$ is the material matrix of concrete and E and G are the elastic modulus and shear modulus, respectively. In the present article, the shear stress components are assumed to be elastic throughout, which is reasonable for most applications failed by concrete cracking or crushing at the fibre level. The compressive behaviour of the normal concrete stress is adopted from Modified Kent and Park model (Park *et al*. 1982) as shown in Fig. 4.

The ascending and descending curves are given by

$$\sigma_c = Kf_c'\left[2\left(\frac{\varepsilon_c}{\varepsilon_0}\right)-\left(\frac{\varepsilon_c}{\varepsilon_0}\right)^2\right], \qquad \text{if} \quad \varepsilon_c \le \varepsilon_0 \tag{27}$$

$$\sigma_c = Kf_c'\left[1-Z(\varepsilon_c-\varepsilon_0)\right] \ge 0.2Kf_c', \qquad \text{if} \quad \varepsilon_0 \le \varepsilon_c \le \varepsilon_u \tag{28}$$

where

$$\varepsilon_0 = 0.002K$$

$$K = 1+\rho_S f_{yh} / f_c'$$

and

$$Z = 0.5\left[\left(3+0.29f_c'\right)\Big/\left(145f_c'-1000\right)+0.75\rho_S\sqrt{h'/S_h}-0.002K\right]^{-0.5}$$

ε_0 is the concrete strain at the maximum stress, ε_u is the concrete ultimate strain in compression, K is a factor which accounts for the strength increase due to confinement, Z is the strain softening slope, f_c' is the concrete compressive cylinder strength in MPa, f_{yh} is the yield strength of stirrups in MPa, ρ_S is the ratio of the volume of hoop reinforcement to the volume of concrete core measured to the external dimensions of stirrups, h' is the width of concrete core measured to the external dimensions of stirrups, and S_h is the centre-to-centre spacing of stirrups or hoop sets. Thus, although the cross section does not explicitly model stirrups, their effect on concrete compressive strength is implicitly considered through the factor K.

Tensile stiffening effect is taken into account by adopting the bilinear stress-strain relationship suggested by Rots *et al*. (1984) as illustrated in Fig. 5 with $\varepsilon_{cr}=f_t'/E_c$, $\varepsilon_{cu}=\alpha_1\varepsilon_{cr}$ and α_1=10~25 (Barzegar-Jamshidi 1987).

The hysteretic behaviour of concrete stress-strain relationship is also considered as shown in Fig. 6. For hysteretic behaviour of concrete in compression, the unloading from a point on the envelop curve takes place along a straight line connecting the point ε_r at which unloading starts to a point ε_p on the strain axis given by Karsan and Jirsa (1969) and Taucer *et al*. (1991) as shown in Eq. (29) and Eq. (30).

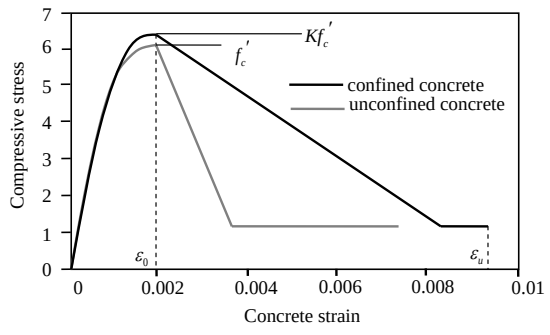

Fig. 4 Stress-strain relationship for concrete under compression

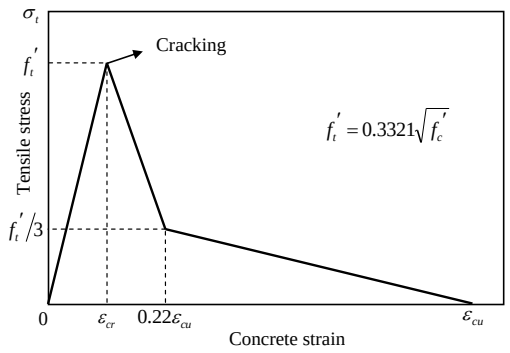

Fig. 5 Stress-strain relationship for concrete under tension

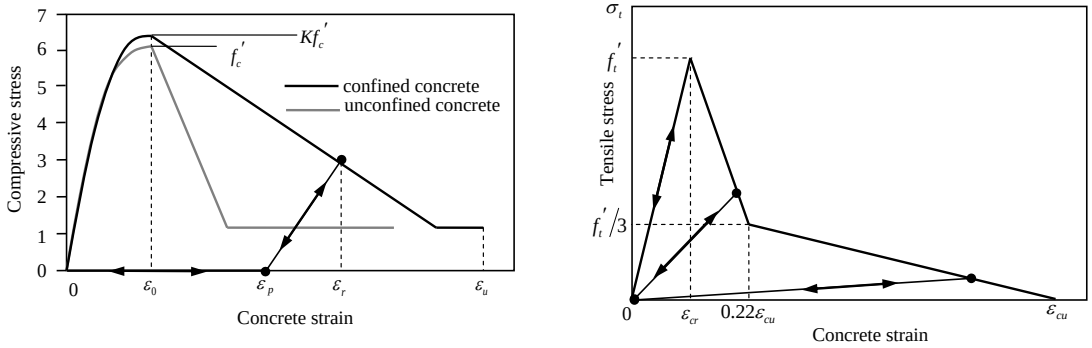

(a) Hysteretic behaviour of concrete in compression (b) Hysteretic behaviour of concrete in tension

Fig. 6 Hysteretic behaviour of confined and unconfined concrete

$$\frac{\varepsilon_p}{\varepsilon_0} = 0.145\left(\frac{\varepsilon_r}{\varepsilon_0}\right)^2 + 0.13\left(\frac{\varepsilon_r}{\varepsilon_0}\right) \quad \text{for} \quad \left(\frac{\varepsilon_r}{\varepsilon_0}\right) < 2 \tag{29}$$

$$\frac{\varepsilon_p}{\varepsilon_0} = 0.707\left(\frac{\varepsilon_r}{\varepsilon_0} - 2\right) + 0.834 \quad \text{for} \quad \left(\frac{\varepsilon_r}{\varepsilon_0}\right) \geq 2 \tag{30}$$

where ε_0 is the strain level corresponding to the maximum compressive stress.

Note that the hysteretic behaviour of concrete in compression and tension above does not account for the cyclic damage of concrete. Additionally, due to the stiffening and softening characteristics of structural deformations, direct displacement-control or load-control method cannot guarantee numerical convergence in all cases with critical points in the load-deflection curves, e.g. limit points and snap-back points. For greater numerical robustness, generalized displacement control method proposed by Yang and Shieh (1990) is employed to ensure stability for iteration at the regions near critical points by self-adaptive loading step sizes and loading directions.

5. Validations

Several examples including steel and RC beams and frames are simulated to test the capabilities of the proposed 3D CR beam element of simulating structural deformations involving geometric and material nonlinearities and the versatility of fibre model.

To demonstrate computational accuracy and efficiency of the proposed CR formulation, total Lagrangian (TL) beam element developed according to Dvorkin *et al*. (1988) is utilized to compare the prediction results by CR formulation for an isolated steel beam with large deformation and a spatial steel frame with material nonlinearity. When simulating large scale structures, computation cost has to be balanced between simulation accuracy and processing time. It is ideal to have fewer elements in structural modelling and yet achieving acceptable accuracy. Therefore, using TL formulations as a benchmark, a case study is conducted for CR beams on the

minimum number of beam elements and the CPU time required for both large deformation and elasto-plastic problems. Besides, I-shaped cross-sections with appropriate fibre schemes are employed to show the capabilities of the proposed CR formulation to predict large deformation and material nonlinear behaviour of steel structures with non-rectangular cross-sections.

For RC structures, the tensile stiffening, compressive softening and hysteretic behaviour of concrete model in CR formulation are taken into consideration, along with the yielding and fracturing behaviour of steel reinforcement. Isolated column and beam members are validated to demonstrate the numerical accuracy and stability of the proposed CR formulation at the member level. At the end, an RC beam-column subassemblage is studied with reliable experimental results. End supports with assembly gaps are calibrated and considered as nonlinear springs in the numerical prediction. In addition to the validations using experimental studies on RC structures, corresponding numerical validations are also conducted by comparing the predictions from the proposed CR beam elements with the simulation results of frame elements provided by the nonlinear finite element software Engineer's Studio (ES) (2009) for isolated RC beams and the ABAQUS solid element (2009) for an RC beam-column subassemblage. These two programs are highly reputable and are expected to produce reliable and accurate predictions for RC beam-column structures.

In order to conduct an objective comparison regarding computational efficiency and prediction accuracy, the TL and CR formulations are studied on the same platform in terms of linear equation solver and data input/output. Moreover, it should be noted that the correctness of the implemented TL beam element formulation is verified against the published simulations by Dvorkin *et al*. (1988) and a great number of others' experimental studies on steel and RC structures.

5.1 A cantilever beam with an end point load

A cantilever beam with an end point load as shown in Fig. 7 is employed to demonstrate the computation accuracy of the proposed CR formulation to simulate problems with large displacement and large rotation. The discretization schemes for the cantilever are two, three and four CR and TL beam elements, respectively. The beam length is 3.0 m and the concentrated load P is 3.11×10^6 N. The material is linear elastic with Young's modulus of 2.1×10^{11} N/m^2. Sixteen fibres are employed to discretize the beam cross-section for both CR and TL elements. Numerical evaluations of elliptic integral solutions of some large deflection problems have been conducted by Mattiasson (1981). The result is utilized to verify the numerical solution from CR beam formulation.

In the comparison with theoretical results as shown in Fig. 8, there is good agreement of the predictions when three and more CR elements are used to mesh the cantilever equally, while the predictions by four TL beam element are not sufficiently accurate. It should be noted that when the cantilever is divided into two elements equally, the CR predictions are still reasonably acceptable. However, the calculation by two TL beam elements cannot predict accurately.

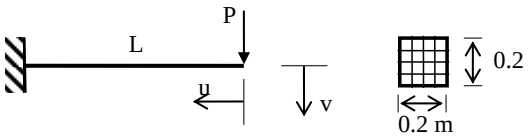

Fig. 7 A cantilever beam with an end point load

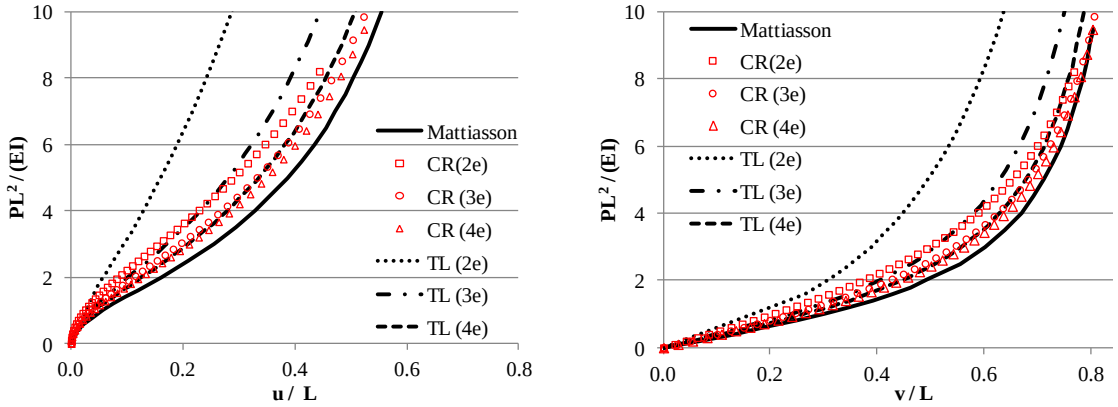

(a) u/L (b) v/L

Fig. 8 The comparison of results for a cantilever beam with an end point load (Mattiasson 1981)

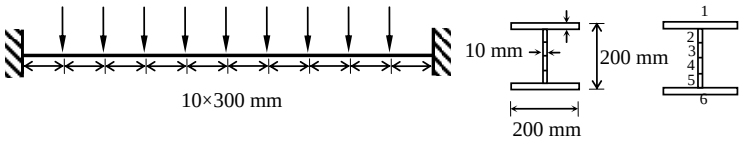

Fig. 9 The finite element idealization and fibre scheme for the I-shaped cross-section

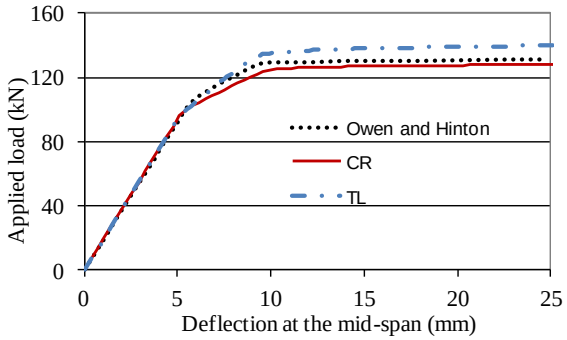

Fig. 10 The relationship of the applied load and the deflection at the mid-span (Hinton and Owen 1984)

5.2 An I-shaped cross-section beam with both ends clamped

To illustrate the versatility of fibre model in CR beam formulation for different cross-sectional shapes, an example of an I-shaped beam with both ends clamped from Owen and Hinton (1984) is shown in Fig. 9. The I-shaped cross-section is discretized into six fibres as shown in Fig. 9 and five CR beam elements are employed to mesh the beam span as the same mesh employed by Owen and Hinton (1984). The material properties are Young's modulus E=210 kN/mm^2, Poisson ratio v=0.3, yield stress σ_0=0.25 kN/mm^2 and strain hardening parameter H=0.

The relationship of the applied load versus central deflection is shown in Fig. 10. Yielding of the cross-section at both clamped ends initiates from flange fibres 1 and 6 and spreads to web fibres 2, 3, 4 and 5. Similarly, the yielding of fibres of the cross-section at the mid-span follows

the same sequence. As shown in Fig. 10, in both the elastic deformation and yielding stages, numerical prediction obtained by CR beam elements agrees well with the results from Owen and Hinton (1984).

A simulation using TL beam elements with the same number of elements and fibre scheme is conducted as well. To achieve the same 25mm mid-span deflection, the computation time for TL formulation is 7.031s and average iteration number for each loading increment is 9 to 11 in the elasto-plastic stage, while CR formulation requires a CPU time of 4.656s and in the elasto-plastic stage average iteration number is only 7 to 8. This represents a computational saving by the proposed CR formulation of more than 30% for elasto-plastic problems. Moreover, with the same mesh and fibre scheme the prediction accuracy of CR formulation is better than those from TL formulation as shown in Fig. 10.

5.3 A space frame with an elasto-perfectly plastic material and different cross-sectional shapes

To demonstrate the capacity of CR formulation to simulate 3D structures using an elasto-perfectly plastic material with different cross-sectional shapes, a space frame with eight members is employed and shown in Fig. 11(a), which was analyzed by Marino (1970), Yang and Fan (1988) and Gendy and Saleeb (1993)based on different approaches. The columns and beams are made of W10×60 and W18×60 sections, respectively. The material properties are E=30,000 ksi (206.9 GPa), G=11,500 ksi (79.3 GPa) and σ_y=34 ksi (234.48 MPa). Each member is of length L = 144 in (3.655 m) with warping restrained at the ends. The member is idealized using two CR beam elements and the cross-section orientations and fibre discretization are illustrated in Fig. 11(b).

The prediction by 16 CR beam elements is shown in Fig. 12 with the comparison of numerical results (Marino 1970, Yang and Fan 1988, Gendy and Saleeb 1993). To demonstrate the advantages in terms of the element number requirement for the proposed CR formulation, the comparisons based on three sets of simulations with each structural member idealized by one, two and three CR and TL elements, respectively, are conducted. Good agreement is achieved by the proposed CR formulation with a small number of elements as shown in Fig. 12. On the other hand,

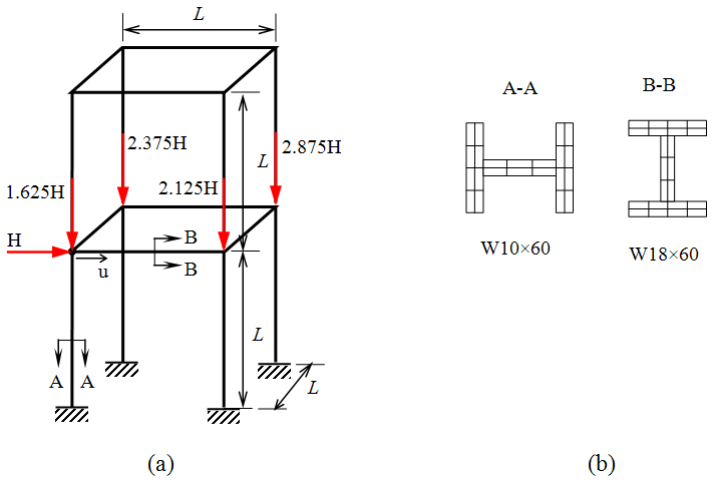

Fig. 11 A space frame with different cross-sectional shapes

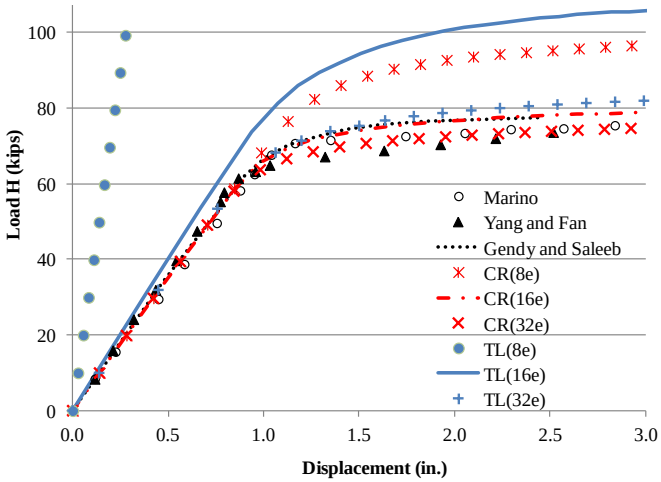

Fig. 12 Curves of Load- horizontal displacement u at the loaded point (Marino 1970, Yang and Fan 1988, Gendy and Saleeb 1993)

Notes: 1 kips=4.448 kN; 1 in.=25.38 mm

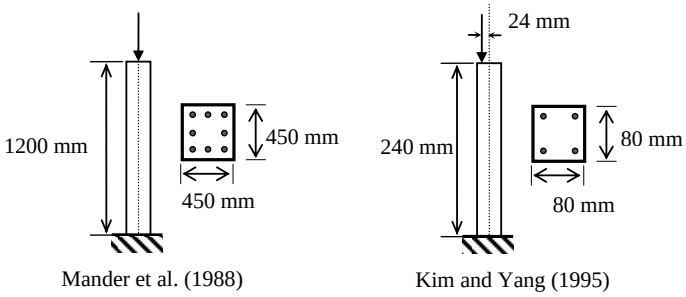

Fig. 13 Reinforced concrete columns

with the same number of beam elements, the simulations by TL formulation demonstrate lower accuracy compared with the results by the proposed CR formulation.

As shown in Fig. 12, the predictions by different numbers of CR elements are quite close, while there is an apparent discrepancy between the predictions by 8, 16 and 32 TL elements. Obviously, compared with TL formulation, there is clear advantage using CR formulation when solving an elasto-plastic problem as the latter requires fewer CR beam elements to produce the same level of accuracy.

5.4 RC columns with concentric or eccentric axial loads

Normal-strength concrete columns subjected to short-term concentric or eccentric axial loads are simulated based on the tests by Mander *et al*. (1988), Kim and Yang (1995). The columns are modelled with six 3-node beam elements. The cross-section was discretized into 100 concrete fibres. The number of steel fibres is equal to the number of steel bars in the column cross-section. Transverse reinforcement is also considered through confined concrete model. The reinforcement is shown in Fig. 13. The column properties are listed in Table 1.

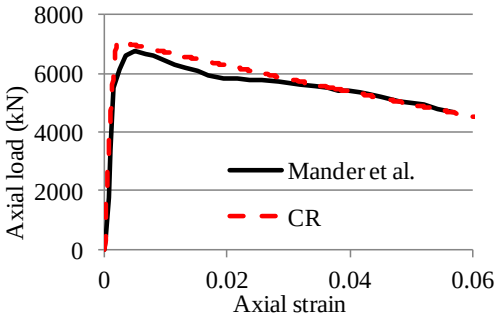

Fig. 14 Result comparisons for an RC column in the test by Mander *et al*. (1988)

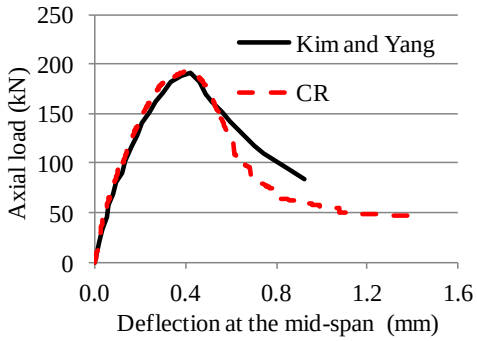

Fig. 15 Result comparisons for an RC column in the test by Kim and Yang (1995)

Table 1 Properties of the RC columns

Column properties	Mander *et al*. (1988)	Kim and Yang (1995)
Column label in the original paper	C6	10M2
Length (mm)	1200	240
Load type (eccentricity)	Concentric	Eccentric (24mm)
Cylinder compressive strength (MPa)	25.3	63.5
Crushing strain of plain concrete	0.002	0.002
Concrete compressive modulus (GPa)	23	33.356
Longitudinal steel ratio (%)	1.79	1.98
Yield stress of longitudinal steel (MPa)	394	387
Yield stress of stirrup (MPa)	309	300
Stirrup transverse volumetric ratio (%)	0.883	0.3
Concrete core width measured to stirrup (mm)	410	62
Stirrup spacing (mm)	72	60

Along with the simulations from experimental studies, the predictions of the proposed CR formulation for both columns subjected to concentric or eccentric axial load are shown in Fig. 14 and Fig. 15, respectively. Excellent agreement for the initial elastic deformation stage is achieved. However, the agreement in the descending parts of both curves are not as good as that for the ascending parts due to the approximation in post-peak descending curves according to the Kent and Park concrete model as discussed in Section 4.2. If the descending slope is calibrated according to the reinforced concrete utilized in the experiment, the proposed CR formulation can provide a closer trend to test results.

5.5 Simply-supported RC beams

Four simply-supported beams with different spans subjected to a concentrated load at the mid-span from the classic set of RC beams tested by Bresler and Scordelis (1963) are simulated using the proposed CR formulation. The geometry, loading, boundary condition and steel reinforcement details are illustrated in Fig. 16. Five elements and 100 concrete fibres are utilized to mesh the beam span and the cross-section. In addition, equivalent steel fibres are assigned to the

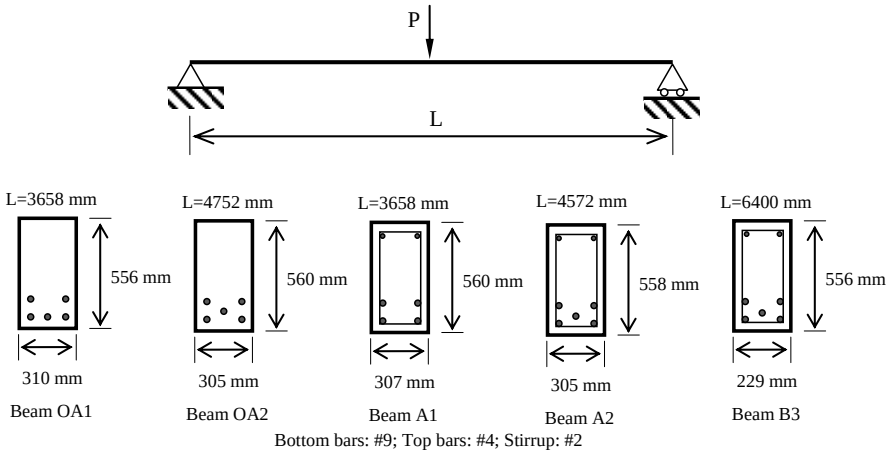

Fig. 16 Geometry and steel reinforcement details of shear beams by Bresler and Scordelis (1963)

Table 2 Material properties of Specimens

Specimen	OA1	OA2	A1	A2	B3
Cylinder compressive strength (MPa)	22.54	23.72	24.06	24.27	38.75
Young's modulus (MPa)	23000	23000	23000	23000	23000
Crushing strain of plain concrete (%)	0.2	0.2	0.2	0.2	0.2
Yield stress of bottom rebars (MPa)	555	555	555	555	552
Yield stress of top rebars (MPa)	-	-	345.41	345.41	345.41
Yield stress of stirrup (MPa)	-	-	325.42	325.42	325.42
Stirrup spacing (mm)	-	-	210	210	190

location of steel reinforcement as shown in Fig. 16. The properties of concrete and steel reinforcement are listed in Table 2.

Since a load-controlled system was used in the experimental study, the post-peak response of the beams was not available and only the initial ascending part was presented. Due to the assumption that the shear stress components always remain elastic for concrete fibres, shear failure in the specimens cannot be captured by the proposed CR formulation. This is a common limitation for current published empirical concrete models. If the shear contribution to concrete failure needs to be taken into account, a three dimensional constitutive material model for concrete should be carried out based on plasticity theory along with concrete fracture. To validate the post-peak loading stage due to flexural failure rather than shear failure, frame element using fibre model in Engineer's Studio (ES) (2009) was employed with Maekawa's nonlinear concrete constitutive relationship (Okamura and Maekawa 1991). The comparison of experimental study and numerical simulations by CR formulation and ES is given in Fig. 17, which shows good agreement in the initial loading stage for all the five specimens. The deflection-load trend from CR and ES are quite close to each other, even though there are some slight discrepancies on the peak strengths.

5.6 An RC subassemblage with nonlinear elastic supports

An RC subassemblage test conducted in NTU by Yu and Tan (2012) is employed to validate

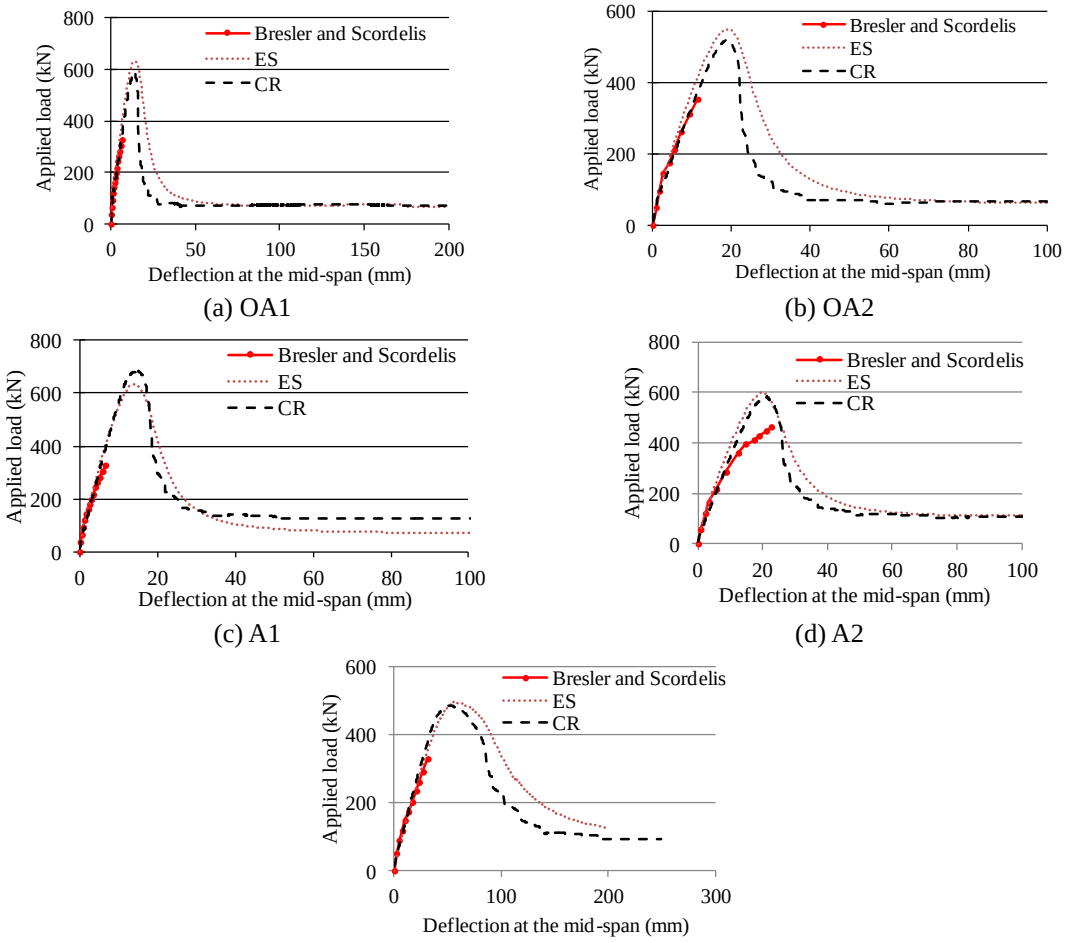

Fig. 17 Comparisons of experimental study and numerical simulations of the RC beams

the proposed CR formulation for the simulation of beam-column structures. The dimensions and steel reinforcement details of the RC subassemblage are shown in Fig. 18(a), in which the beam section is 250 mm×150 mm and its net span is 5750 mm. 31 CR elements are employed to mesh the sub-assemblage as illustrated in Fig. 18(b). It should be noted that the reinforcement configuration along the beam is symmetric but not uniform. The material properties of concrete and steel reinforcement are listed in Table 3 and Table 4, respectively.

For the accuracy of numerical simulations, the measured stiffness and assembly gap measured at the specimen supports connected with the end column stubs in the test have been calibrated and converted into nonlinear spring elements at compression and tension zones as shown in Fig. 19. The calibration results are given in Table 5.

With consideration of nonlinear spring elements at the specimen supports, a simulation is conducted using ABAQUS 6.9 (2009) by the solid element C3D8R (an 8-node linear brick with reduced integration) which is expected to produce a reliable and accurate prediction for large scale RC beam-column structures. To stabilize the numerical simulation, explicit solver is employed

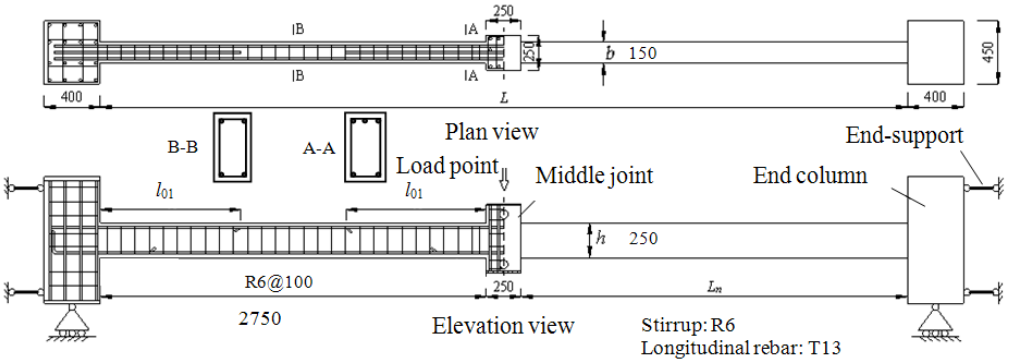

(a) Dimensions and reinforcement details of the RC subassemblage (unit in mm)

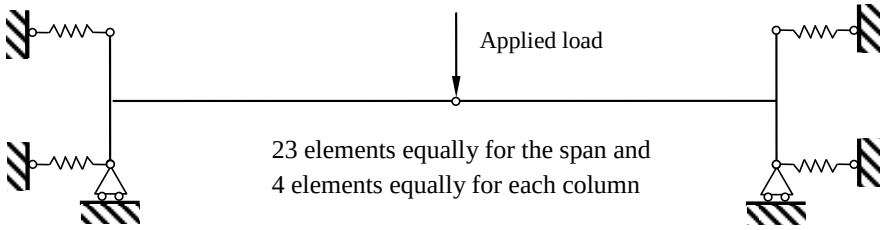

(b) Numerical model

Fig. 18 Detailing and the boundary conditions of the RC subassemblage (mm)

Table 3 Material properties of concrete

Tensile strength f_t (MPa)	Compressive strength f_c' (MPa)	Strain at compressive strength ε_{c0} (%)	Initial modulus of elasticity Ec (MPa)
3.5	38.2	0.25	29645

Table 4 Material properties of steel reinforcement

Rebar type	Nominal diameter (mm)	Yield strength f_y (MPa)	Elastic modulus E_s (MPa)	Tensile strength f_u (MPa)	Ultimate strain ε_u (%)	Hardening modulus E_h (MPa)
R6	10	349	199177	459	--	--
T13	13	494	185873	593	10.92	929.2086

Table 5 Calibration for the end-supports in the laboratory

Horizontal restraints	Tension stiffness (kN/m)	Compression stiffness (kN/m)	Tension gap (mm)	Compression gap (mm)
Top	62413.11	--	2.4	--
Bottom	23050.53	146390.7	4.1	-0.7

during the displacement-control loading procedure. A comparison of experimental study and numerical simulations by proposed CR formulation and ABAQUS 6.9 is illustrated in Fig. 20.

Both sets of numerical simulations provide good approximations for the initial loading stage and catenary action stage after the bottom rebars fracture at the mid-span. However, the simulation by ABAQUS fails to capture the peak strength and rebar fracture phenomenon in terms of the

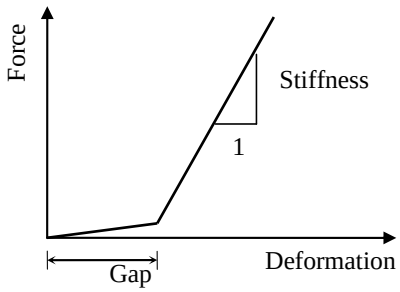

Fig. 19 Nonlinear behaviour of the proposed spring element to simulate the specimen supports

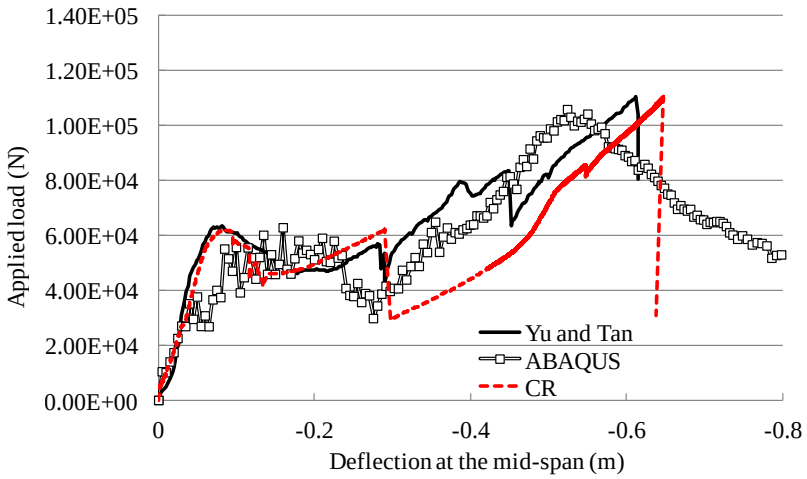

Fig. 20 Result comparisons for the RC subassemblage

sudden decrease in the loading versus deformation curve due to the 'embedment constraint' technique between concrete and steel reinforcement. Even though fibre model of the proposed CR formulation also assumes perfect bonding between concrete and reinforcement, the rebar fracture can still be simulated when integrating the internal force vector and stiffness matrix around the cross-section with fibres.

6. Conclusions

Based on 3-node 3D CR beam elements using vectorial rotational variables, fibre model and material nonlinearity in terms of elasto-plastic incremental stress-strain relationship for both steel and concrete are derived and conducted. The derivations on the local internal force vector and stiffness matrix are generalized into cross-sections without symmetry. Different cross-sectional shapes and reinforced concrete cross-sections can be conveniently discretized into a combination of fibres with various areas and material properties for steel and concrete regions. In the utilized concrete model, compressive concrete behaviour is described by Modified Kent and Park model, while tensile stiffening effect is also taken into account.

With the advantages of proposed CR formulation with fibre model, the calculations for stress and strain of steel and concrete fibres and the element pure deformation decoupled from a rigid-body movement are conducted in the local coordinate system. The predictions by the proposed CR formulation for both steel and RC structures are accurate and efficient for large displacement and large rotation problems and elasto-plastic problems with the comparison of TL formulation and ABAQUS solid element.

Through several numerical examples and validations with test results, the proposed co-rotational 3D beam element demonstrates satisfactory numerical capacity when analyzing both steel and RC structures with arbitrary cross-sectional shapes undergoing geometric and material nonlinearities. The proposed CR beam formulation can be an effective approach to simulate the deformation of steel and RC framed structures in the process of progressive collapse.

References

Abaqus/Standard user's manual 6.9.1 (2009), Hibbit, Karlsson & Sorensen, Inc., Pawtucket, Rhode Island, U.S.

Barzegar-Jamshidi, F. (1987), "Non-linear finite element analysis of re-inforced concrete under short term monotonic loading", University of Illinois at Urbana-Champaign, USA.

Bathe, K.J. and Bolourchi, S. (1979), "Large displacement analysis of three-dimensional beam structures", *Int. J. Numer. Method. Eng*., **14**(7), 961-986.

Battini, J.M. (2008), "A non-linear corotational 4-node plane element", *Mech. Res. Commun*., **35**(6), 408-413.

Bresler, B. and Scordelis, A.C. (1963), "Shear strength of RC beams", *ACI J*., **60**(1), 51-74.

Cardona, A. and Geradin, M. (1988), "A beam finite element non-linear theory with finite rotations", *Int. J. Numer. Method. Eng*., **26**(11), 2403-2438.

Crisfield, M.A. (1990), "A consistent co-rotational formulation for non-linear, three-dimensional, beam-elements", *Comput. Meth. Appl. Mech. Eng*., **81**(2), 131-150.

Dvorkin, E.N., Onte, E. and Oliver, J. (1988), "On a non-linear formulation for curved Timoshenko beam elements considering large displacement/rotation increments", *Int. J. Numer. Method. Eng*., **26**(7), 1597-1613.

Engineer's Studio User' s help 1.00.01 (2009), FORUM8 Co., Ltd., Japan.

Felippa, C.A. and Haugen, B. (2005), "A unified formulation of small-strain corotational finite elements: I. Theory", *Comput. Meth. Appl. Mech. Eng*, **194**(21-24), 2285-2335.

Gendy, A.S. and Saleeb, A.F. (1993), "Generalized yield surface representations in the elasto-plastic three-dimensional analysis of frames", *J. Comput. Struct*., **49**(2), 351-362.

Hinton, E. and Owen, D.R.J. (1984), "Finite element software for plates and shells", University College, Swansea, U.K.

Hsiao, K.M., Horng, H.J. and Chen, Y.R. (1987), "A corotational procedure that handles large rotations of spatial beam structures", *Comput. Struct*., **27**(6), 769-781.

Karsan, I.D. and Jirsa, J.O. (1969), "Behavior of concrete under compressive loadings", *J. Struct. Div*., ASCE, **95**(ST12), 2543-2563.

Kim, J.K. and Yang, J.K. (1995), "Buckling behaviour of slender high-strength concrete columns", Eng. Struct., **17**(1), 39-51.

Li, Z.X. (2007), "A co-rotational formulation for 3D beam element using vectorial rotational variables", Comput. Mech., **39**(3), 309-322.

Mander, J.B., Priestley, M.J.N. and Par, R. (1988), "Observed stress-strain behavior of confined concrete", *J. Struct. Eng*., ASCE **114**(8), 1827-1849.

Marino, S. (1970), "Analysis of space frames", Thesis presented to Lehigh University, Bethlehem, PA.

partial fulfillment of the requirements for the degree of Doctor of Philosophy.
Mattiasson, K. (1981), "Numerical results from large deflection beam and frame problems analysed by means of elliptic integrals", *Int. J. Numer. Method. Eng*, **17**(1), 145-153.
Nanakorn, P. and Vu, L.N. (2006), "A 2D field-consistent beam element for large displacement analysis using the total Lagrangian formulation", *Finite Elem. Anal. Des*., **42**(14-15), 1240-1247.
Okamura, H. and Maekawa, K. (1991), *Nonlinear analysis and constitutive models of reinforced concrete*, Giho-do Press, University of Tokyo, Japan.
Park, R., Negel Priestley, M.J. and Gill, W.D. (1982), "Ductility of square-confined concrete columns", *J. Struct. Div*., ASCE, **108**(4), 929-950.
Rots, J.G., Kusters, G.M.A. and Blaauwendraad, J. (1984), "The need for fracture mechanics options in finite element models for concrete structures", *Proceedings of international conference on Computer Aided Analysis and Design of Concrete Structures Part 1*, Pineridge Press, Swansea, U.K.
Schulz, M. and Filippou, F.C. (2001), "Non-linear spatial Timoshenko beam element with curvature interpolation", *Int. J. Numer. Method. Eng*, **50**(4), 761-785.
Taucer, F.F., Spacone, E. and Filippou, F.C. (1991), "A fiber beam-column element for seismic response analysis of reinforced concrete structures", Earthquake Engineering Research Center, University of California, Berkeley
Teh, L. and Clarke, M. (1999), "Symmetry of tangent stiffness matrices of 3D elastic frame", *J. Eng. Mech*., **125**(2), 248-251.
Yang, Y.B. and Fan, H.T. (1988), "Yield surface modeling of I-sections with nonuniform torsion", *J. Eng. Mech*., ASCE, **114**(6), 953-972.
Yang, Y.B. and Shieh, M.S. (1990), "Solution method for nonlinear problems with multiple critical points", *AIAA J*., **28**(12), 2110-2116.
Yu, J. and Tan, K.H. (2012), "Structural behavior of reinforced concrete beam column sub-assemblages under a middle column removal scenario", *J. Struct. Div*., ASCE.

Abbreviations

TL= Total Lagrangian
UL = Updated Lagrangian
CR = Co-rotational
RC = Reinforced concrete
ES= Engineer's Studio

Notations

$\mathbf{a}$	Flow vector
$\mathbf{e}_{iy}$, $\mathbf{e}_{iz}$	Direction vectors in the global system of Node i
e_{iy,n_i} , e_{iy,m_i} , e_{iz,n_i}	Global vectorial rotational variables of Node i
$\mathbf{f}_L$	Internal force vector in the local system
f_c'	Concrete compressive cylinder strength
f_t'	Concrete tensile strength in the cylinder splitting test
f_{yh}	Yield strength of stirrups
h_i	Lagrangian interpolation function
h'	Width of concrete core measured to the external dimensions of stirrups

k_0	Shear factor of cross-sections
m	User-defined iteration number
$\mathbf{r}_{iy}$, $\mathbf{r}_{iz}$	Direction vectors in the local system of Node i
r_{iy,n_i} , r_{iy,m_i} , r_{iz,n_i}	Local vectorial rotational variables of Node i
$\mathbf{t}_i$	Displacement vector at any point in the beam element
$\mathbf{u}_G$	Degrees of freedom in the global system
$\mathbf{u}_L$	Degrees of freedom in the local system
u_i, v_i, w_i	Local displacements of Node i
x, y, z	Local coordinate system
A	Cross-sectional area of a CR beam
$\mathbf{B}$	Geometric matrix
$\mathbf{D}$	Material matrix
$\mathbf{D}_{ep}$	Equivalent material matrix
E	Elastic modulus of steel
E_c	Elastic modulus of concrete
F	Yield function of steel
G	Shear modulus of steel
H	Strain hardening parameter of steel
$\mathbf{K}_L$	Stiffness matrix in the local system
K	Confinement factor in concrete model
L	Length of a CR beam
$\mathbf{P}$	External load
R	Ratio of the part outside the yield surface to the whole stress increment
S_h	Centre-to-centre spacing of stirrups or hoop sets
X_1, X_2, X_3	Global coordinate system
U_i, V_i, W_i	Global displacements of Node i
V	Volume of a CR beam element
Z	Strain softening slope in concrete model
$d\boldsymbol{\sigma}$	Incremental stress vector
$d\boldsymbol{\sigma}^{(0)} \sim d\boldsymbol{\sigma}^{(5)}$	Components of incremental stress
$d\boldsymbol{\sigma}_e$	Whole stress increment of steel
σ_y	Yield stress of steel
$d\boldsymbol{\varepsilon}$	Incremental strain vector
$\boldsymbol{\varepsilon}$	Green strain
$\boldsymbol{\varepsilon}^{(0)} \sim \boldsymbol{\varepsilon}^{(5)}$	Components of Green strain
ε_0	Concrete strain at the maximum compressive stress
ε_{cr}	Concrete strain at the maximum tensile stress
ε_{cu}	Concrete ultimate strain in tension
ε_r	Unloading start point
ε_p	Unloading end point the strain axis
ε_u	Concrete ultimate strain in compression
ρ_S	Ratio of the volume of hoop reinforcement to the volume of concrete core measured to the external dimensions of stirrups
ζ	Natural coordinate system along the centre line of the beam element

Appendix. A

$$\mathbf{f}_0 = \mathbf{B}^{(0)^{\mathrm{T}}}\mathbf{D}\boldsymbol{\varepsilon}^{(0)}$$

$$\mathbf{f}_1 = \mathbf{B}^{(1)^{\mathrm{T}}}\mathbf{D}\boldsymbol{\varepsilon}^{(0)} + \mathbf{B}^{(0)^{\mathrm{T}}}\mathbf{D}\boldsymbol{\varepsilon}^{(1)}$$

$$\mathbf{f}_2 = \mathbf{B}^{(2)^{\mathrm{T}}}\mathbf{D}\boldsymbol{\varepsilon}^{(0)} + \mathbf{B}^{(0)^{\mathrm{T}}}\mathbf{D}\boldsymbol{\varepsilon}^{(2)}$$

$$\mathbf{f}_3 = \mathbf{B}^{(3)^{\mathrm{T}}}\mathbf{D}\boldsymbol{\varepsilon}^{(0)} + \mathbf{B}^{(0)^{\mathrm{T}}}\mathbf{D}\boldsymbol{\varepsilon}^{(3)} + \mathbf{B}^{(2)^{\mathrm{T}}}\mathbf{D}\boldsymbol{\varepsilon}^{(1)} + \mathbf{B}^{(1)^{\mathrm{T}}}\mathbf{D}\boldsymbol{\varepsilon}^{(2)}$$

$$\mathbf{f}_4 = \mathbf{B}^{(4)^{\mathrm{T}}}\mathbf{D}\boldsymbol{\varepsilon}^{(0)} + \mathbf{B}^{(1)^{\mathrm{T}}}\mathbf{D}\boldsymbol{\varepsilon}^{(1)} + \mathbf{B}^{(0)^{\mathrm{T}}}\mathbf{D}\boldsymbol{\varepsilon}^{(4)}$$

$$\mathbf{f}_5 = \mathbf{B}^{(5)^{\mathrm{T}}}\mathbf{D}\boldsymbol{\varepsilon}^{(0)} + \mathbf{B}^{(2)^{\mathrm{T}}}\mathbf{D}\boldsymbol{\varepsilon}^{(2)} + \mathbf{B}^{(0)^{\mathrm{T}}}\mathbf{D}\boldsymbol{\varepsilon}^{(5)}$$

$$\mathbf{f}_6 = \mathbf{B}^{(3)^{\mathrm{T}}}\mathbf{D}\boldsymbol{\varepsilon}^{(1)} + \mathbf{B}^{(1)^{\mathrm{T}}}\mathbf{D}\boldsymbol{\varepsilon}^{(3)} + \mathbf{B}^{(2)^{\mathrm{T}}}\mathbf{D}\boldsymbol{\varepsilon}^{(4)} + \mathbf{B}^{(4)^{\mathrm{T}}}\mathbf{D}\boldsymbol{\varepsilon}^{(2)}$$

$$\mathbf{f}_7 = \mathbf{B}^{(5)^{\mathrm{T}}}\mathbf{D}\boldsymbol{\varepsilon}^{(1)} + \mathbf{B}^{(1)^{\mathrm{T}}}\mathbf{D}\boldsymbol{\varepsilon}^{(5)} + \mathbf{B}^{(2)^{\mathrm{T}}}\mathbf{D}\boldsymbol{\varepsilon}^{(3)} + \mathbf{B}^{(3)^{\mathrm{T}}}\mathbf{D}\boldsymbol{\varepsilon}^{(2)}$$

$$\mathbf{f}_8 = \mathbf{B}^{(5)^{\mathrm{T}}}\mathbf{D}\boldsymbol{\varepsilon}^{(4)} + \mathbf{B}^{(3)^{\mathrm{T}}}\mathbf{D}\boldsymbol{\varepsilon}^{(3)} + \mathbf{B}^{(4)^{\mathrm{T}}}\mathbf{D}\boldsymbol{\varepsilon}^{(5)}$$

$$\mathbf{f}_9 = \mathbf{B}^{(4)^{\mathrm{T}}}\mathbf{D}\boldsymbol{\varepsilon}^{(4)}$$

$$\mathbf{f}_{10} = \mathbf{B}^{(5)^{\mathrm{T}}}\mathbf{D}\boldsymbol{\varepsilon}^{(5)}$$

$$\mathbf{f}_{11} = \mathbf{B}^{(4)^{\mathrm{T}}}\mathbf{D}\boldsymbol{\varepsilon}^{(1)} + \mathbf{B}^{(1)^{\mathrm{T}}}\mathbf{D}\boldsymbol{\varepsilon}^{(4)}$$

$$\mathbf{f}_{12} = \mathbf{B}^{(5)^{\mathrm{T}}}\mathbf{D}\boldsymbol{\varepsilon}^{(2)} + \mathbf{B}^{(2)^{\mathrm{T}}}\mathbf{D}\boldsymbol{\varepsilon}^{(5)}$$

$$\mathbf{f}_{13} = \mathbf{B}^{(4)^{\mathrm{T}}}\mathbf{D}\boldsymbol{\varepsilon}^{(3)} + \mathbf{B}^{(3)^{\mathrm{T}}}\mathbf{D}\boldsymbol{\varepsilon}^{(4)}$$

$$\mathbf{f}_{14} = \mathbf{B}^{(5)^{\mathrm{T}}}\mathbf{D}\boldsymbol{\varepsilon}^{(3)} + \mathbf{B}^{(3)^{\mathrm{T}}}\mathbf{D}\boldsymbol{\varepsilon}^{(5)}$$

Appendix. B

$$\mathbf{K}_0 = \mathbf{B}^{(0)^{\mathrm{T}}}\mathbf{D}\mathbf{B}^{(0)} + \boldsymbol{\varepsilon}^{(0)^{\mathrm{T}}}\mathbf{D}\frac{\partial \mathbf{B}^{(0)}}{\partial \mathbf{u}_L}$$

$$\mathbf{K}_1 = \mathbf{B}^{(1)^{\mathrm{T}}}\mathbf{D}\mathbf{B}^{(0)} + \boldsymbol{\varepsilon}^{(1)^{\mathrm{T}}}\mathbf{D}\frac{\partial \mathbf{B}^{(0)}}{\partial \mathbf{u}_L} + \mathbf{B}^{(0)^{\mathrm{T}}}\mathbf{D}\boldsymbol{\varepsilon}^{(1)} + \boldsymbol{\varepsilon}^{(0)^{\mathrm{T}}}\mathbf{D}\frac{\partial \mathbf{B}^{(1)}}{\partial \mathbf{u}_L}$$

$$\mathbf{K}_2 = \mathbf{B}^{(2)^{\mathrm{T}}}\mathbf{D}\mathbf{B}^{(0)} + \boldsymbol{\varepsilon}^{(2)^{\mathrm{T}}}\mathbf{D}\frac{\partial \mathbf{B}^{(0)}}{\partial \mathbf{u}_L} + \mathbf{B}^{(0)^{\mathrm{T}}}\mathbf{D}\mathbf{B}^{(2)} + \boldsymbol{\varepsilon}^{(0)^{\mathrm{T}}}\mathbf{D}\frac{\partial \mathbf{B}^{(2)}}{\partial \mathbf{u}_L}$$

$$\mathbf{K}_3 = \mathbf{B}^{(3)^{\mathrm{T}}}\mathbf{D}\mathbf{B}^{(0)} + \boldsymbol{\varepsilon}^{(3)^{\mathrm{T}}}\mathbf{D}\frac{\partial \mathbf{B}^{(0)}}{\partial \mathbf{u}_L} + \mathbf{B}^{(0)^{\mathrm{T}}}\mathbf{D}\mathbf{B}^{(3)} + \boldsymbol{\varepsilon}^{(0)^{\mathrm{T}}}\mathbf{D}\frac{\partial \mathbf{B}^{(3)}}{\partial \mathbf{u}_L}$$
$$+ \mathbf{B}^{(2)^{\mathrm{T}}}\mathbf{D}\mathbf{B}^{(1)} + \boldsymbol{\varepsilon}^{(2)^{\mathrm{T}}}\mathbf{D}\frac{\partial \mathbf{B}^{(1)}}{\partial \mathbf{u}_L} + \mathbf{B}^{(1)^{\mathrm{T}}}\mathbf{D}\mathbf{B}^{(2)} + \boldsymbol{\varepsilon}^{(1)^{\mathrm{T}}}\mathbf{D}\frac{\partial \mathbf{B}^{(2)}}{\partial \mathbf{u}_L}$$

$$\mathbf{K}_4 = \mathbf{B}^{(4)^{\mathrm{T}}}\mathbf{D}\mathbf{B}^{(0)} + \boldsymbol{\varepsilon}^{(4)^{\mathrm{T}}}\mathbf{D}\frac{\partial \mathbf{B}^{(0)}}{\partial \mathbf{u}_L} + \mathbf{B}^{(1)^{\mathrm{T}}}\mathbf{D}\mathbf{B}^{(1)} + \boldsymbol{\varepsilon}^{(1)^{\mathrm{T}}}\mathbf{D}\frac{\partial \mathbf{B}^{(1)}}{\partial \mathbf{u}_L} + \mathbf{B}^{(0)^{\mathrm{T}}}\mathbf{D}\mathbf{B}^{(4)} + \boldsymbol{\varepsilon}^{(0)^{\mathrm{T}}}\mathbf{D}\frac{\partial \mathbf{B}^{(4)}}{\partial \mathbf{u}_L}$$

$$\mathbf{K}_5 = \mathbf{B}^{(5)^{\mathrm{T}}}\mathbf{D}\mathbf{B}^{(0)} + \boldsymbol{\varepsilon}^{(5)^{\mathrm{T}}}\mathbf{D}\frac{\partial \mathbf{B}^{(0)}}{\partial \mathbf{u}_L} + \mathbf{B}^{(2)^{\mathrm{T}}}\mathbf{D}\mathbf{B}^{(2)} + \boldsymbol{\varepsilon}^{(2)^{\mathrm{T}}}\mathbf{D}\frac{\partial \mathbf{B}^{(2)}}{\partial \mathbf{u}_L} + \mathbf{B}^{(0)^{\mathrm{T}}}\mathbf{D}\mathbf{B}^{(5)} + \boldsymbol{\varepsilon}^{(0)^{\mathrm{T}}}\mathbf{D}\frac{\partial \mathbf{B}^{(5)}}{\partial \mathbf{u}_L}$$

$$\mathbf{K}_6 = \mathbf{B}^{(3)^{\mathrm{T}}}\mathbf{D}\mathbf{B}^{(1)} + \boldsymbol{\varepsilon}^{(3)^{\mathrm{T}}}\mathbf{D}\frac{\partial \mathbf{B}^{(1)}}{\partial \mathbf{u}_L} + \mathbf{B}^{(1)^{\mathrm{T}}}\mathbf{D}\mathbf{B}^{(3)} + \boldsymbol{\varepsilon}^{(1)^{\mathrm{T}}}\mathbf{D}\frac{\partial \mathbf{B}^{(3)}}{\partial \mathbf{u}_L} + \mathbf{B}^{(2)^{\mathrm{T}}}\mathbf{D}\mathbf{B}^{(4)} + \boldsymbol{\varepsilon}^{(2)^{\mathrm{T}}}\mathbf{D}\frac{\partial \mathbf{B}^{(4)}}{\partial \mathbf{u}_L} + \mathbf{B}^{(4)^{\mathrm{T}}}\mathbf{D}\mathbf{B}^{(2)} + \boldsymbol{\varepsilon}^{(4)^{\mathrm{T}}}\mathbf{D}\frac{\partial \mathbf{B}^{(2)}}{\partial \mathbf{u}_L}$$

$$\mathbf{K}_7 = \mathbf{B}^{(5)^{\mathrm{T}}}\mathbf{D}\mathbf{B}^{(1)} + \boldsymbol{\varepsilon}^{(5)^{\mathrm{T}}}\mathbf{D}\frac{\partial \mathbf{B}^{(1)}}{\partial \mathbf{u}_L} + \mathbf{B}^{(1)^{\mathrm{T}}}\mathbf{D}\mathbf{B}^{(5)} + \boldsymbol{\varepsilon}^{(1)^{\mathrm{T}}}\mathbf{D}\frac{\partial \mathbf{B}^{(5)}}{\partial \mathbf{u}_L} + \mathbf{B}^{(2)^{\mathrm{T}}}\mathbf{D}\mathbf{B}^{(3)} + \boldsymbol{\varepsilon}^{(2)^{\mathrm{T}}}\mathbf{D}\frac{\partial \mathbf{B}^{(3)}}{\partial \mathbf{u}_L} + \mathbf{B}^{(3)^{\mathrm{T}}}\mathbf{D}\mathbf{B}^{(2)} + \boldsymbol{\varepsilon}^{(3)^{\mathrm{T}}}\mathbf{D}\frac{\partial \mathbf{B}^{(2)}}{\partial \mathbf{u}_L}$$

$$\mathbf{K}_8 = \mathbf{B}^{(5)^{\mathrm{T}}}\mathbf{D}\mathbf{B}^{(4)} + \boldsymbol{\varepsilon}^{(5)^{\mathrm{T}}}\mathbf{D}\frac{\partial \mathbf{B}^{(4)}}{\partial \mathbf{u}_L} + \mathbf{B}^{(3)^{\mathrm{T}}}\mathbf{D}\mathbf{B}^{(3)} + \boldsymbol{\varepsilon}^{(3)^{\mathrm{T}}}\mathbf{D}\frac{\partial \mathbf{B}^{(3)}}{\partial \mathbf{u}_L} + \mathbf{B}^{(4)^{\mathrm{T}}}\mathbf{D}\mathbf{B}^{(5)} + \boldsymbol{\varepsilon}^{(4)^{\mathrm{T}}}\mathbf{D}\frac{\partial \mathbf{B}^{(5)}}{\partial \mathbf{u}_L}$$

$$\mathbf{K}_9 = \mathbf{B}^{(4)^{\mathrm{T}}}\mathbf{D}\mathbf{B}^{(4)} + \boldsymbol{\varepsilon}^{(4)^{\mathrm{T}}}\mathbf{D}\frac{\partial \mathbf{B}^{(4)}}{\partial \mathbf{u}_L}$$

$$\mathbf{K}_{10} = \mathbf{B}^{(5)^{\mathrm{T}}}\mathbf{D}\mathbf{B}^{(5)} + \boldsymbol{\varepsilon}^{(5)^{\mathrm{T}}}\mathbf{D}\frac{\partial \mathbf{B}^{(5)}}{\partial \mathbf{u}_L}$$

$$\mathbf{K}_{11} = \mathbf{B}^{(4)^{\mathrm{T}}}\mathbf{D}\mathbf{B}^{(1)} + \boldsymbol{\varepsilon}^{(4)^{\mathrm{T}}}\mathbf{D}\frac{\partial \mathbf{B}^{(1)}}{\partial \mathbf{u}_L} + \mathbf{B}^{(1)^{\mathrm{T}}}\mathbf{D}\mathbf{B}^{(4)} + \boldsymbol{\varepsilon}^{(1)^{\mathrm{T}}}\mathbf{D}\frac{\partial \mathbf{B}^{(4)}}{\partial \mathbf{u}_L}$$

$$\mathbf{K}_{12} = \mathbf{B}^{(5)^{\mathrm{T}}}\mathbf{D}\mathbf{B}^{(2)} + \boldsymbol{\varepsilon}^{(5)^{\mathrm{T}}}\mathbf{D}\frac{\partial \mathbf{B}^{(2)}}{\partial \mathbf{u}_L} + \mathbf{B}^{(2)^{\mathrm{T}}}\mathbf{D}\mathbf{B}^{(5)} + \boldsymbol{\varepsilon}^{(2)^{\mathrm{T}}}\mathbf{D}\frac{\partial \mathbf{B}^{(5)}}{\partial \mathbf{u}_L}$$

$$\mathbf{K}_{13} = \mathbf{B}^{(4)^{\mathrm{T}}}\mathbf{D}\mathbf{B}^{(3)} + \boldsymbol{\varepsilon}^{(4)^{\mathrm{T}}}\mathbf{D}\frac{\partial \mathbf{B}^{(3)}}{\partial \mathbf{u}_L} + \mathbf{B}^{(3)^{\mathrm{T}}}\mathbf{D}\mathbf{B}^{(4)} + \boldsymbol{\varepsilon}^{(3)^{\mathrm{T}}}\mathbf{D}\frac{\partial \mathbf{B}^{(4)}}{\partial \mathbf{u}_L}$$

$$\mathbf{K}_{14} = \mathbf{B}^{(5)^{\mathrm{T}}}\mathbf{D}\mathbf{B}^{(3)} + \boldsymbol{\varepsilon}^{(5)^{\mathrm{T}}}\mathbf{D}\frac{\partial \mathbf{B}^{(3)}}{\partial \mathbf{u}_L} + \mathbf{B}^{(3)^{\mathrm{T}}}\mathbf{D}\mathbf{B}^{(5)} + \boldsymbol{\varepsilon}^{(3)^{\mathrm{T}}}\mathbf{D}\frac{\partial \mathbf{B}^{(5)}}{\partial \mathbf{u}_L}$$